Universidade de Aveiro
2018/2019

Departamento de Biologia

Nuno Tiago Fidalgo Tavares

Radium-223 in metastatic prostate cancer: effects on metastasis microenvironment

Rádio-223 no cancro da próstata metastático: efeitos no microambiente metastático

DECLARAÇÃO

Declaro que este relatório é integralmente da minha autoria, estando devidamente referenciadas as fontes e obras consultadas, bem como identificadas de modo claro as citações dessas obras. Não contém, por isso, qualquer tipo de plágio quer de textos publicados, qualquer que seja o meio dessa publicação, incluindo meios eletrónicos, quer de trabalhos académicos.

Universidade de Aveiro
2018/2019

Departamento de Biologia

Nuno Tiago Fidalgo Tavares

Radium-223 in metastatic prostate cancer: effects on metastasis microenvironment

Rádio-223 no cancro da próstata metastático: efeitos no microambiente metastático

Dissertação apresentada à Universidade de Aveiro para cumprimento dos requisitos necessários à obtenção do grau de Mestre em Biologia Molecular e Celular, realizada sob a orientação científica da Professora Doutora Salomé Pires Lourenço, Professora Auxiliar da Faculdade de Medicina da Universidade de Coimbra e co-orientação da Professora Doutora Virgília Azevedo Silva, Professora Auxiliar do Departamento de Biologia da Universidade de Aveiro.

"Progress is made by trial and failure; the failures are generally a hundred times more numerous than the successes ; yet they are usually left unchronicled."

Sir William Ramsay

O júri

Presidente: Professor Doutor Mário Guilherme Garcês Pacheco, Professor Auxiliar c/Agregação, Universidade de Aveiro

Vogal - Arguente Principal: Doutor Paulo Nuno Centeio Matafome, Professor Adjunto, Instituto Politécnico de Coimbra - Escola Superior de Tecnologia de Saúde de Coimbra

Vogal - Orientador: Professora Doutora Ana Salomé dos Santos Pires Lourenço, Professora Assistente, Faculdade de Medicina da Universidade de Coimbra

Agradecimentos

À Professora Doutora Maria Filomena Botelho, Professora Catedrática da Faculdade de Medicina da Universidade de Coimbra e diretora do Serviço de Biofísica da mesma instituição, por me ter acolhido na sua equipa, pela disponibilidade, apoio, partilha de conhecimento científico e pelas críticas construtivas na revisão do manuscrito.

À Professora Doutora Ana Salomé Pires, orientadora desta dissertação, por todo o apoio, disponibilidade, amizade, simpatia, entusiamo e pela motivação, até quando eu andava a "bater com a cabeça" com os resultados. Por todo o incentivo e pela contribuição essencial que deu neste trabalho, quer no dia a dia quer na revisão, ajuda preciosa na análise estatística e pela correção da dissertação, mesmo quando o tempo era escasso.

À Professora Doutora Virgília Silva, orientadora interna desta dissertação, pela ajuda quando foi necessário e pelo apoio e disponibilidade.

À Professora Doutora Margarida Abrantes, pela amizade, simpatia e por me ter aceitado no projeto, mesmo apesar das circunstâncias. O meu muito obrigado por todos os conselhos, partilha de conhecimentos e experiência científica, e pelas críticas construtivas na dissertação.

À Professora Doutora Mafalda Laranjo, pela disponibilidade constante, por todos os ensinamentos, partilha de conhecimentos e pela ajuda preciosa nas experiências de microscopia.

Ao Mestre Paulo Teixeira, por todos os conselhos e sugestões para o trabalho, por ser incansável, estar sempre disponível em qualquer altura e por toda a imensa ajuda na imunocitoquímica e na obtenção das imagens morfológicas.

Ao Serviço de Medicina Nuclear do Centro Hospitalar e Universitário de Coimbra, dirigido pela Dra. Gracinda Costa, pela doação do radiofármaco ^{223}Ra.

Ao Mestre Ricardo Teixo, por toda a ajuda, pelos conselhos e ensinamentos no laboratório, que me foram bastante úteis.

Ao Zé, por ser um companheiro de gabinete exemplar e tornar as horas no laboratório mais leves e animadas.

À Mestre Catarina Guilherme, à Soraia, Ana Rita e Catarina Ferreira, por tornarem o dia a dia no laboratório e as horas de almoço mais alegres, e por toda a ajuda sempre que necessário.

Ao grupo que me acompanha já desde a licenciatura, Zé, Tércia, David, Fábio e Magalhães, pela amizade e por todas as peripécias vividas na vida académica, o meu muito obrigado.

Aos colegas do Mestrado em BMC, especialmente ao Oldair, à Bárbara e à Mariana, pela amizade, o meu obrigado por partilharem o primeiro ano comigo.

Aos meus amigos que já vêm desde há mais tempo, o Luís Pedro e o Márcio, e a todos aqueles que vêm desde o secundário, por todos os momentos vividos e pela amizade que há-de perdurar.

Aos meus avôs maternos, Fausto e Guida, que partiram demasiado cedo, por me ajudarem a tornar a pessoa que sou hoje, e que espero que estejam orgulhosos de mim. Palavras nunca serão suficientes para agradecer. Também aos meus avós paternos, Olímpio e Quitas, pelos ensinamentos e experiência de vida transmitida sempre.

A toda a minha família, os que estão perto e os que por alguma razão estão mais longe, o meu bem-haja.

À Vera, por todo o amor e por me ter aturado todos os dias, nos bons e nos maus momentos, por toda a motivação, carinho e apoio dados ao longo desta etapa. Sem dúvida que não tenho como agradecer todo o apoio incondicional que me deste juntamente com o Flash, e que este ano foste um dos meus pilares.

À minha irmã Beatriz, por todos os bons momentos que já vivemos, pela boa disposição, alegria e tagarelice que demonstra sempre, e porque apesar de todas as birras e chatices é e será sempre uma das pessoas mais importantes da minha vida.

Aos meus pais, Nuno e Teresa, as pessoas mais importantes da minha vida. Por todos os sacrifícios que fizeram e que fazem todos os dias, pois sem vocês nada disto seria possível. A educação e os valores que me transmitiram desde que nasci e todo o apoio que demonstraram desde o primeiro dia foram sem dúvida a maior motivação que podia ter tido. O meu muito obrigado por terem apostado em mim sempre e especialmente depois das dúvidas deste último ano, sem qualquer hesitação que tudo isto é por vocês.

Palavras-chave: cancro da próstata, culturas celulares 3D, Rádio-223, microambiente tumoral

Resumo: O cancro da próstata é a segunda neoplasia mais frequente em homens e a quinta causa de morte relacionada com cancro em todo o mundo. A terapia de privação de andrógenos tem sido o *gold standard* para o tratamento do cancro da próstata avançado, mas apesar desta terapia ser associada com a remissão do tumor, é também associada com a recorrência do cancro na próstata, que pode levar a um estádio mais avançado da doença designado cancro da próstata resistente à castração. Apesar deste ser ainda um estádio mortal da doença, hoje em dia existem algumas opções terapêuticas para aumentar a sobrevida e providenciar maior qualidade de vida aos doentes. Uma destas opções é o Rádio-223, um radiofármaco emissor de partículas alfa que tem um efeito positivo na taxa de sobrevivência dos doentes, e também na diminuição de eventos sintomáticos relacionados com o esqueleto. Sendo assim, os principais objetivos deste trabalho experimental foram a otimização e caracterização de um modelo celular em três dimensões de duas linhas celulares de cancro da próstata, e a avaliação dos efeitos do Rádio-223 no modelo tridimensional utilizando diversas técnicas de biologia molecular e celular.

Na primeira fase do trabalho, utilizou-se o método de levitação magnética para a formação de esferóides tridimensionais de PC3 e LnCap, utilizando-se posteriormente o ensaio MTT para verificar a influência do modelo no metabolismo celular, microscopia de fluorescência e colorações histoquímicas para estudar a estrutura e viabilidade dos esferóides, imunocitoquímica para a expressão proteica e citometria de fluxo para avaliar a viabilidade e as vias de morte celular. Os efeitos do Rádio-223 foram estudados posteriormente pelo ensaio SRB, para avaliar o conteúdo proteico total, por *Alamar Blue*, para estudar a proliferação celular, e pela coloração May-Grünwald-Giemsa, para avaliação da morfologia celular pós-irradiação.

As duas linhas celulares demonstraram formar diferentes tipos de estruturas tridimensionais em cultura, e por formarem estruturas mais compactas, decidiu-se estudar a linha celular PC3. As estruturas das células PC3 demonstraram ter uma conformação esférica e apresentaram extensas zonas necróticas e apoptóticas, visto que os esferóides possuíam dimensões na ordem dos mm^2. Além disso, os esferóides exibiram diferenças na expressão de algumas proteínas chave quando comparadas com células controlo em monocamada, facto que deve também ser tido em conta no estudo de terapêuticas para o cancro com este tipo de modelos.

Após a irradiação dos esferóides com Rádio-223, todas as doses testadas apresentaram uma diminuição comparadas com o controlo, quer em conteúdo proteico total ou proliferação celular. Os resultados mostraram também que o tratamento com Rádio-223 exibiu menor eficácia nos esferóides quando comparados com células em monocamada, o que se pode dever ao facto das estruturas tridimensionais serem modelos mais próximos do cenário in vivo, e, portanto, a citotoxicidade do Rádio-223 poderá ser diminuída. Além disso, como as partículas alfa têm baixo alcance de penetração e o esferóide tem um tamanho consideravelmente grande, o radiofármaco pode não penetrar com eficácia na estrutura tridimensional.

Assim, com este estudo foi possível concluir que, como expectável, o Rádio-223 atua de forma diferente quando testado em monocamada e em culturas tridimensionais, e que é de grande importância avaliar este, e no futuro outros fármacos, com culturas em três dimensões, pois estas podem funcionar como uma "ponte" entre os estudos *in vitro* em monocamada e os estudos *in vivo*, melhor mimetizando o microambiente tumoral.

Keywords: prostate cancer, Radium-223, 3D cell culture, tumor microenvironment

Abstract: Prostate cancer is the second most frequent neoplasia in males and the fifth cancer-related cause of death worldwide. Androgen deprivation therapy has been the gold standard treatment for advanced prostate cancer. However, in spite of this therapy being associated with the tumour's remission, it is also associated with prostate cancer recurrence, which leads to a lethal stage of the disease named castration resistant prostate cancer. Despite the high mortality of this stage, nowadays there are some therapy options to manage it, raising survival and providing more life quality to the patients. One of these options is the Radium-223, an alpha particle emitter radiopharmaceutical that has a positive effect on the increasing of overall survival of patients, also lowering the risk of symptomatic skeletal events.

The main objectives of this experimental work were to optimize and characterize a three-dimensional cell culture model in two prostate cancer cell lines and then assess the effects of the Radium-223 on the model through molecular and cellular techniques.

In the first phase of the work, it was used the magnetic levitation method in order to form three-dimensional spheroids of PC3 and LnCap, using after the MTT assay to check the PC3 model's influence on the cells metabolism, fluorescence microscopy and histochemical staining techniques to study spheroid structure and viability, immunocytochemistry for protein expression and flow cytometry to learn about the culture's viability and cell death pathways. The effects of the Radium-223 were then studied by the SRB assay, to evaluate total protein content, by Alamar Blue, to study cell proliferation, and by May-Grünwald-Giemsa staining, to check cellular morphology post-irradiation.

The two different cell lines showed different types of three-dimensional structures in culture, and due to its more compact and spherical structure, it was decided to study the PC3 cell line in this experimental work. The PC3 structures displayed a spherical conformation and presented extensive necrotic and apoptotic zones, since the size of the spheroid was in the order of mm^2. Besides, the spheroids also exhibited different expression in some key proteins when compared with control cells cultured in monolayer, an important fact when testing cancer therapeutics.

After the irradiation of the spheroids with Radium-223, all doses tested presented a decrease compared to the control whether it was in total protein content or cell proliferation. The results also showed that the Radium-223 treatment exhibited a lower efficacy in the spheroids when compared with monolayer cells, which can be due to the fact that the three-dimensional structures are closer to mimicking the *in vivo* scenario, and so the cytotoxicity of the Radium-223 is decreased. Also, as alpha particles have low penetration ranges and the spheroid has a large size, the radiopharmaceutical might not be properly entering the three-dimensional structure.

Thereby, with this work it was possible to conclude that, as expected, the Radium-223 acts differently when tested in monolayer and in three dimensional cultures, as shown by the primary results obtained. Thus, it is very important to evaluate this and, in the future, other drugs or radiopharmaceuticals, using *in vitro* three dimensional spheroids before passing to *in vivo* studies, as they can function as a bridge between the two and give more information than standard cell culture, better mimicking the tumor microenvironment.

Contents

Resumo: ..... **i**

..... **iii**

Abstract: ..... **iii**

Contents ..... **v**

List of Figures ..... **vii**

List of Tables ..... **x**

Abbreviations ..... **xi**

CHAPTER 1 - INTRODUCTION **1**

1.1. Prostate Cancer 3

1.1.1. Epidemiology 4

1.1.2. Risk Factors 6

1.1.3. Diagnosis 7

1.1.4. Grading and Staging 8

1.1.5. Treatment 11

1.2. Advanced Prostate Cancer and Androgen Dependence 12

1.3. Castration-resistant Prostate Cancer 13

1.3.1. Radium-223 in the treatment of metastatic castration-resistant prostate cancer 15

1.4. Cancer Microenvironment and 3D Cultures 20

CHAPTER 2 - OBJECTIVES **25**

CHAPTER 3 – MATHERIAL AND METHODS **29**

3.1. Cell Culture 31

3.2. Establishment of Prostate Cancer 3D Cell Cultures 32

3.3. Irradiation of Prostate Cancer 3D spheroids with Radium-223 34

3.4. Analysis of Protein Content by the Sulforhodamine B (SRB) assay 35
3.5. Cell Proliferation Analysis by Alamar Blue Assay 36
3.6. Cell Metabolism Evaluation by MTT Assay 37
3.7. Morphology Studies by the May-Grünwald-Giemsa Staining 37
3.8. Histological Staining 38
3.8.1. Haematoxylin and Eosin (H & E) 38
3.8.2. Toluidine Blue 39
3.9. Protein Markers Presence by Immunocytochemistry 39
3.10. Structure and Cell Viability Characterization by Fluorescence Microscopy 40
3.11. Cell Death Populations and Viability Studies by Flow Cytometry 40
3.12. Statistical Analysis 41
CHAPTER 4 - RESULTS 43
4.1. Spheroids Characterization 45
4.1.1. Spheroid evolution over time 45
4.1.2. Influence of the Magnetic Levitation Method on Cell Metabolism 47
4.1.3. Spheroid Structure 48
4.1.4. Protein Markers Presence 50
4.1.5. Cell Viability and Death Populations 51
4.2. Treatment of Spheroids with Radium-223 54
4.2.1. Cell Proliferation 54
4.2.2. Protein Content 55
4.2.3. Cell Morphology 56
CHAPTER 5 - DISCUSSION 57
CHAPTER 6 – CONCLUSIONS AND FUTURE PERSPECTIVES 57
CHAPTER 7 - REFERENCES 57

List of Figures

Figure 1: Prostate anatomical location in the male reproductive system (Adapted from Prostate Cancer Centre, 2016). 3
Figure 2: Zonal anatomy of the prostate (Adapted from Sathianathen et al, 2018). 4
Figure 3: Initiation and progression of malignant prostate transformation (Adapted from Shen and Abate-Shen, 2010). 4
Figure 4: Comparison between World and Portugal cancer incidence and mortality in 2018, for both sexes, all ages (Adapted from GLOBOCAN 2018). 5
Figure 5: Gleason scoring system, from 1 (least aggressive) to 5 (most aggressive) (Adapted from Prostate Cancer Foundation of Australia). 9
Figure 6: TNM system for prostate cancer staging (Adapted from American Joint Committee on Cancer). 10
Figure 7: The 2015 CUA-CUOG Guidelines for the management of castration-resistant prostate cancer (CRPC) (Adapted from Saad et al., 2015). 14
Figure 8: Mechanism of action of Ra-223 on a tissue and molecular scale (Adapted from Deshayes et al., 2017). 17
Figure 9: Decay chain of Radium-223. (Taken from Marques et al., 2018). 18
Figure 10: The 5 steps of metastasis: invasion, intravasation, survival, extravasation and secondary tumor development (Adapted from Sleeboom et al., 2018). 21
Figure 11: Scheme representing complexity versus technique (in vitro and in vivo) (Adapted from Caicedo-Carvajal et al., 2012). 22
Figure 12: Spheroid tumor model and principal characteristics (Adapted from Sant and Johnston, 2017). 24
Figure 13: Magnetic nanoparticle used in the magnetic levitation method. 32
Figure 14: Levitating drive used to attract the cells with magnets after the inoculation with the magnetic nanoparticle (A) and spheroid formed after the application of the MLM (B). 33
Figure 15: Concentrating drive, used to change the medium of the 3D cultures. 33
Figure 16: Alamar blue reaction in the cellular environment (Adapted from Bionity.com). 36

Figure 17: Representative images of PC3 3D spheroid arrangement and growing at 0 (a), 1 (b), 2 (c), 3 (d), 4 (e), 5 (f) and 6 (g) days after seeding. Images were all taken at 40x magnification and the scale at a) is equal to 1 mm. 45
Figure 18: Growth curve of PC3 spheroids according to their areas. The arrow represents the time when only one compact spheroid is formed instead of various cell clustering. Results are expressed as mean and standard error of the mean (SEM) from n=6 of at least 3 independent experiments. Wilcoxon and Tukey test (*** $p < 0.001$, * $p < 0.05$)..... 46
Figure 19: Representative images of LnCap 3D cultures clustering and growing at 1 (a), 2 (b) and 5 (c) days after seeding. Images were all taken at a 40x magnification. 46
Figure 20: Evaluation of the cell's metabolic activity after the incubation with the magnets and NS. Data is normalized to the control and expressed as mean and SEM from n>6 of at least 3 independent experiments. Wilcoxon and Mann-Whitney U tests (*** $p < 0.001$, ** $p < 0.01$, * $p < 0.05$). 47
Figure 21: PC3 3D spheroid stained with toluidine blue with 40x (a) and 400x (b) magnifications. 48
Figure 22: PC3 3D spheroid smear stained with haematoxylin and eosin with 40x (a) and 400x (b) magnifications. 49
Figure 23: Representative images of spheroid structure in PC3 3D structures (a, b, d) when compared to cells cultured in monolayer (c). a) and b) were stained with DAPI, and c) and d) were stained with DAPI and CellMask for membrane. Images were taken in a fluorescence microscope with 40x (a), 100x (b) and 200x (c, d) magnifications..... 49
Figure 24: Immunohistochemical staining on 2D monolayer (a, c, e, g, i) and 3D spheroid (b, d, f, h, j) cell culture. The illustrated samples were stained for Ki-67 (a, b), p16 (c, d), caspase 3 (e, f), vimentin (g, h) and p53 (i, j). Images were taken using an optic microscope with 100x and 200x magnification. 50
Figure 25: Representative images of DAPI (a), AnV (b) and PI (c) stained 2D monolayer cultured PC3 cells. Images were taken in a fluorescence microscope with 100x magnification. 52
Figure 26: Representative images of merged (a), DAPI (b), AnV (c) and PI (d) stained 3D spheroid PC3 cells. Images were taken in a fluorescence microscope with 100x magnification. 52

Figure 27: Viability and cell death pathways evaluation by flow cytometry. The results were obtained with PC3 7-day monolayer cultured cells (2D) and spheroids (3D). The results are expressed as percentage of viable cells, in apoptosis, late apoptosis/necrosis and necrosis, and present mean and SEM from n>6 from at least 3 independent experiments. Mann-Whitney U Test (*** $p < 0.001$)..... 53
Figure 28: Evaluation of the cell viability by the Alamar Blue assay 48 hours after the irradiation with ^{223}Ra with doses of 1, 4, 10, 15 and 20 mGy both in monolayer cells (2D) and spheroids (3D). Results are normalized to control and expressed as mean and SEM from n>9 from at least 3 independent experiments (2D is only n=3 from 1 independent experiment). Wilcoxon test (** $p < 0.01$, * $p < 0.05$) 54
Figure 29: Evaluation of the protein content by the SRB assay 48 hours after the irradiation with ^{223}Ra with a dose of 10 mGy both in monolayer cells (2D) and spheroids (3D). Results are normalized to control and expressed as mean and SEM from n>9 from at least 3 independent experiments. T student test and t one sample test (*** $p < 0.001$) 55
Figure 30: Representative images (400x) of morphologic features in PC3 spheroid cells post irradiation with ^{223}Ra, after cells staining by May-Grünwald-Giemsa staining. Control (a), 1 mGy (b), 4 mGy (c) and 10 mGy (d)..... 56

List of Tables

Table 1: Doses, initial activities and times used in the irradiation with Radium-223. 35

Table 2: Antibodies used in the immunocytochemistry studies and characteristics (clone, incubation time, dilution and provider). 40

Table 3: Resume of the immunocytochemical staining pattern: positive staining (++), mild staining (+) and minor to negative staining (-). 51

Abbreviations

207Pb - Lead-207

223Ra - Radium-223

2D - two-dimensional

3D - three-dimensional

AA - abiraterone acetate

ADT - androgen deprivation therapy

ALSYMPCA - Alpharadin in Symptomatic Prostate Cancer

AnV - Annexin V

AR - androgen receptor

ATCC - American Type Culture Collection

ATM - ATM serine/threonine kinase

BRCA1 - breast cancer predisposition gene 1

BRCA2 - breast cancer predisposition gene 2

CHEK2 - checkpoint kinase 2

CRPC - castration-resistant prostate cancer

DAB - 3,3′-Diaminobenzidine

DAPI - 4,6-diamidino-2-phenylindole

DHT - 5α-dihydrotestosterone

DNA - deoxyribonucleic acid

DRE - digital rectal examination

ECM - extracellular matrix

EMA - European Medicines Agency

FBS - Fetal Bovine Serum

FDA - Food and Drug Administration

FITC - Fluorescein isothiocyanate

GnRH - gonadotropin-releasing hormone

Gy - Gray

H & E - Haematoxylin and Eosin

HIF1-α - Hypoxia-inducible factor 1-alpha

LET - linear energy transfer

mCRPC - metastatic castration-resistant prostate cancer

MLH1 - mutL homolog 1

MLM - magnetic levitation method

MSH1 - mismatch repair ATPase 1

MSH2 - mismatch repair ATPase 2

MSH6 - mismatch repair ATPase 6

MTT - 3-(4,5-dimethylthiazolyl-2)2,5-diphenyltetrazolium bromide

NS - NanoShuttle

PAP - prostate acid phosphatase

PBS - Phosphate Buffer Saline

PFA - paraformaldehyde

PI - propidium iodide

PSA - prostate specific antigen

RPMI - Roswell Park Memorial Institute

ROS - Reactive Oxygen Species

SEM - standard error of the mean

SRB - sulforhodamine B

TNM - tumor-node-metastasis system

TRUS - transrectal ultrasound

USA - United States of America

CHAPTER 1 - INTRODUCTION

1.1. Prostate Cancer

Cancer is a complex and heterogeneous group of diseases with multiple molecular parts characterized by uncontrolled growth and propagation of cells disrespecting the boundaries of tissues, which has the possibility of locoregional spread and distant metastasis (American Cancer Society, 2016; Moses et al., 2018).

The prostate is the largest accessory gland in the male reproductive system. Anatomically, it is essentially walnut sized, it surrounds the urethra at the pelvic cavity, and it can be found immediately inferior to the bladder, posterior to the pubic symphysis and anterior to the rectum (Figure 1). Secretions from the prostate, associated with secretions from the seminal vesicles, contribute for the formation of the semen during the ejaculation (Moore, 2013; Drake et al., 2015).

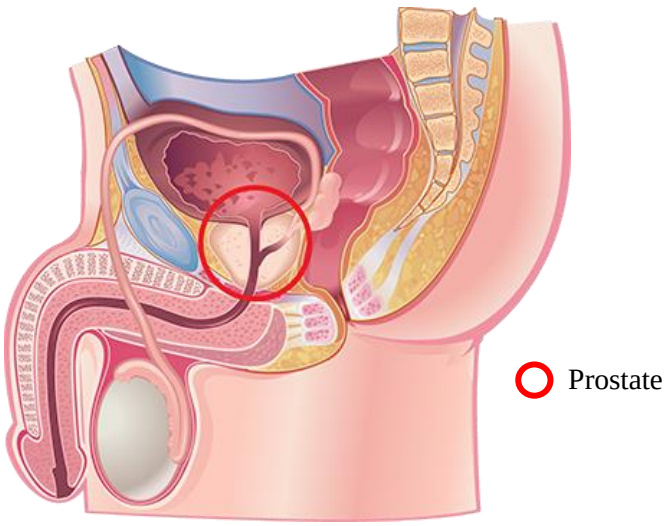

Figure 1: Prostate anatomical location in the male reproductive system (Adapted from Prostate Cancer Centre, 2016).

This organ normally measures 3 x 3 x 5 cm, has a volume of 25 mL and is an aggregate of 30 to 50 tubuloalveolar glands arranged in three concentric layers, the inner mucosal layer, the intermediate submucosal layer and the peripheral layer (Pallwein et al., 2008). The prostate is surrounded by a fibroelastic capsule that is rich in smooth muscle. There are two types of glands in the prostate, periurethral submucosal glands and main prostatic glands in the periphery. The glandular epithelium is pseudostratified columnar with numerous secretory granules, whose products include acid phosphatase, citric acid fibrinolysin and other proteins (Aaron et al., 2016).

In 1988, McNeal proposed a model for the prostate's zonal anatomy (Figure 2), where it is divided into four regions, the anterior fibromuscular stroma, the central zone, the transitional zone and the peripheral zone (McNeal, 1981). About 70% of all prostate cancers are originated on the peripheral zone, while 20% from transitional zone and about 10% from the central zone (Pallwein et al., 2008).

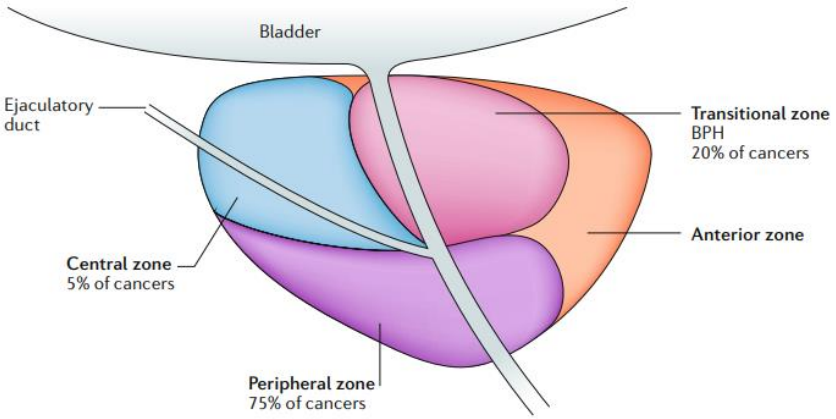

Figure 2: Zonal anatomy of the prostate (Adapted from Sathianathen et al, 2018).

The malignant transformation of the prostate follows a process with multiple steps, as it can be seen in Figure 3. It initiates as a prostatic intraepithelial neoplasia that disturbs the normal prostate tissue, and if left untreated, progress to a localized prostate cancer, which progresses to a prostate adenocarcinoma with locoregional invasion, and that ends as a metastatic prostate cancer (Wang et al., 2018).

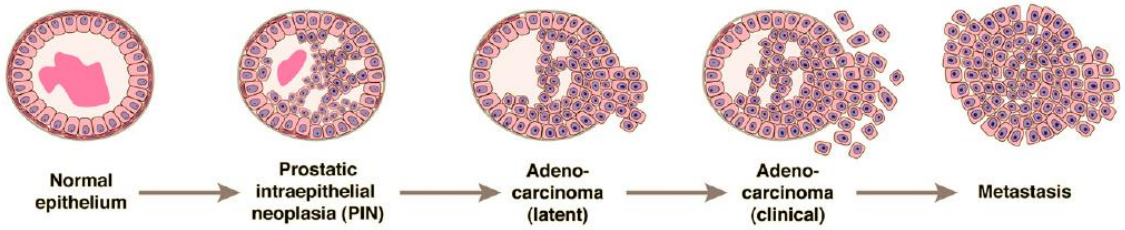

Figure 3: Initiation and progression of malignant prostate transformation (Adapted from Shen and Abate-Shen, 2010).

1.1.1. Epidemiology

It is estimated that there will be 1.3 million cases of prostate cancer in 2018 and approximately 359 000 deaths associated with the disease, making it the second most

frequent type of cancer and the fifth cancer associated cause of the death in males (Bray et al., 2018).

Prostate cancer is the most frequently diagnosed cancer among men in more than half of the countries worldwide, being more common in the Americas, Northern and Western Europe, Oceania and most of the Sub-Saharan Africa. It is also the most common cancer cause of death in males at 46 countries, most of them in the Sub-Saharan Africa and the Caribbean (Bray et al., 2018).

Regarding Portugal (Figure 4), prostate cancer is the second most incident cancer considering both sexes, only behind breast cancer, and the first among men. In terms of mortality, it has been decreasing over the last years as it has been in most developed countries, due to improvement in care and advancements in diagnosis, staging and treatment (Bray et al., 2018).

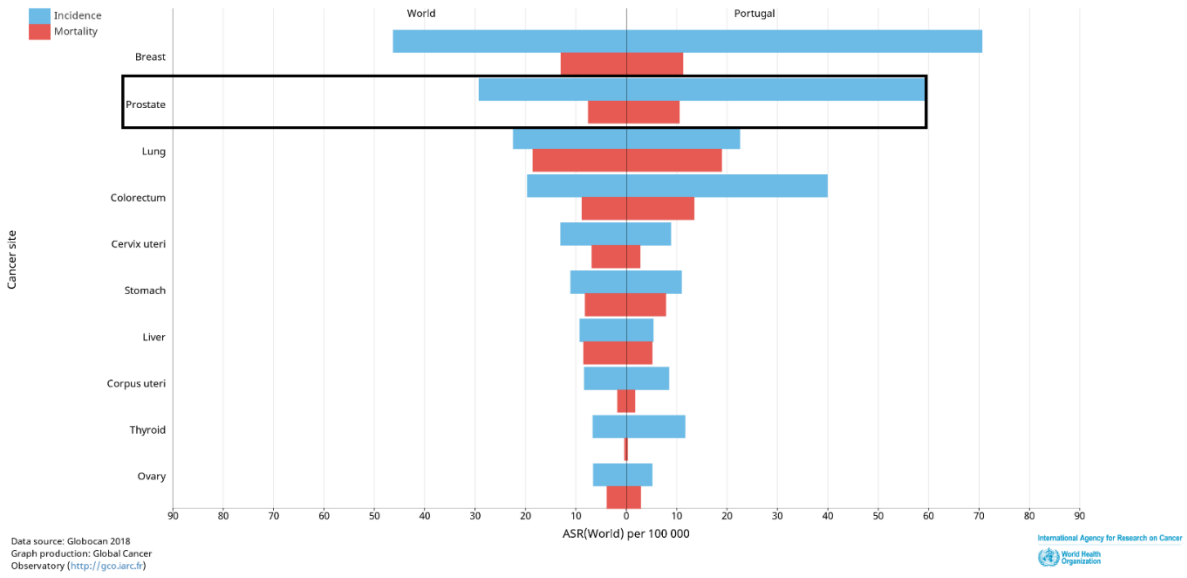

Figure 4: Comparison between World and Portugal cancer incidence and mortality in 2018, for both sexes, all ages (Adapted from GLOBOCAN 2018).

Statistics point to higher incidence of prostate cancer on African men in the United States of America (USA) and the Caribbean, which reflects an ethnic and genetic predisposition. However, the disease's etiology is still not well described, as there are very few risk factors truly associated with advanced prostate cancer besides body fat, for which there is convincing association. Prostate cancer is also the commonest cancer affecting men of African descent (Eeles and Raghallaigh, 2018).

Mortality for this type of cancer has been lowering in many countries, namely in North America, Oceania, Western Europe and in the more developed Asian countries. In

contrast, there has been a raise in mortality in Central and South America, Asia and Eastern Europe, which is possibly linked to an increment of risk factors in combination with limited access to adequate treatment (Bray et al., 2018).

1.1.2. Risk Factors

There are several risk factors associated with prostate cancer such as age, ethnicity, genetics, and some environmental and lifestyle causes. In spite of this, the origin of the disease is still poorly understood due to its complexity and heterogeneity. The most preponderant factor related to prostate cancer is age, because it has extremely low incidence on men under 50 years of age, which make only approximately 0.1% of all patients, and about 85% of all cases are diagnosed on patients that are older than 65 (Patel and Klein, 2009).

There also seems to be a relationship between ethnicity and prostate cancer, as the incidence of the disease is about 60% higher and the mortality rate raises 2 to 3 times in African American men when compared to Caucasian men (Powell and Bollig-Fischer, 2013).

Prostate cancer can be divided into 3 types: sporadic, familial or hereditary. The disease has been shown to cluster in families and to exhibit patterns of Mendelian heritage. The familial cases refer to the ones in which a man has one or more direct family members affected by the disease, and the hereditary cases to a set of cases in a family that show a distribution pattern consistent with Mendelian heritage of a susceptibility gene (Patel and Klein, 2009). Sporadic cancers make 85% of all cases (Carter et al., 1992).

Concerning genetics, high-risk prostate cancer predisposition genes exist, with carriers of a rare missense mutation (G84E) in the HOXB13 gene having a 33% risk of developing prostate cancer (Ewing et al., 2012). The protein coded by the HOXB13 gene plays an important role in urogenital development and has high expression levels in the normal prostate (Pilie et al., 2016).

Germline deleterious mutations in breast cancer predisposition gene 2 (BRCA2) also increase the risk of developing prostate cancer by 20% in a lifetime, whereas mutations in breast cancer predisposition gene 1 (BRCA1) have also been reported and raise the risk of the disease in 9.5% by an age of 65 years. Both of these are tumour suppressor genes, are

linked to deoxyribonucleic acid (DNA) response and repair processes and their loss of function is associated with a deficiency on the repair of DNA double-strand (Castro and Eeles, 2012). Mutations in other genes involved in DNA repair processes such as ATM serine/threonine kinase (ATM), checkpoint kinase 2 (CHEK2), mismatch repair ATPases 1, 2 and 6 genes (MSH1, MSH2 and MSH6) and mutL homolog 1 (MLH1) have been associated with risk of developing prostate cancer as well, although they are not as preponderant as BRCA1 and BRCA2 (Eeles and Raghallaigh, 2018).

1.1.3. Diagnosis

Digital rectal examination (DRE) is the primary test for the initial clinical assessment of the prostate, being routinely used along the prostate specific antigen (PSA) testing (Adhyam and Gupta, 2012). Rectal examination has the advantage of being able to detect non-secreting PSA tumors but, according to studies made about its accuracy, its predicting value is about 50%, failing to detect a substantial number of cancers. When compared with PSA test, it detects them in a pathologically more advanced stage (Borley and Feneley, 2009).

The PSA, also called kallikrein-3, is a serine protease that was first described in 1979 (Wang et al., 2017). It is produced by the prostatic epithelium and by the periurethral glands, being present in large quantities in the prostatic secretions, however it is released into the bloodstream as a consequence of disruption in normal prostate epithelium (Shen and Abate-Shen, 2010). Its functions, being a protease, comprise liquefying semen, promoting sperm motility and dissolving cervical mucus. As a biomarker, the PSA is organ-specific but not cancer-specific, which means that besides cancer, it can also detect prostate benign epithelial masses, fact that lowers its specificity as a prostate cancer detection test (Ohori et al., 1995). Population studies have demonstrated that PSA normal levels tend to raise with age. In the USA, the mortality rate for prostate cancer has lowered for almost half since the beginning of PSA testing, more than 25 years ago. The PSA test is simple and safe, but it is not completely efficient because of its high false positive rate, because it can be raised by conditions like ejaculation, bacterial prostatitis or acute urinary retention (Adhyam and Gupta, 2012).

Transrectal ultrasound (TRUS) is nowadays the most common technique used to diagnose prostate cancer (Borley and Feneley, 2009). It is very useful because it allows to guide needle biopsies and to map specific regions of the prostate. This technique is also a well-tolerated procedure by patients with low incidence of significant complications. The pre-indications to proceeding with TRUS-guided biopsies include abnormal DRE, and an elevated or increasing PSA (Lopes et al., 2015).

1.1.4. Grading and Staging

The grade of a cancer shows how and how fast a cancer might grow, whereas the stage shows how far the cancer has spread. Normal tissues have a normal and ordered growth pattern but in cancer tissues, this growth pattern is not ordered, because cancer cells have unpredictable and unlimited growth. Based on this principle Donald Gleason, in 1966, developed a method to grade and score prostatic adenocarcinomas. This system is based on the histological appearance of the prostate cancer cells taken from biopsies, more specifically on the extent of gland differentiation and stromal growth pattern (Chen and Zhou, 2016). As it can be seen in Figure 5, Gleason 1 represents the most differentiated and is associated with better prognosis, and Gleason 5 denotes the less differentiated ones and is related with poor prognosis.

The final result of the Gleason biopsy scoring system corresponds to the sum of two components, the degree of the predominant pattern and the degree of the secondary pattern, which means the scoring can go from a minimum of 2 to a maximum of 10.

The development of the Gleason score and subsequent modifications made by the International Society of Urological Pathology in 2005 and 2014 allowed the establishment of a more accurate prediction of prognosis in prostate cancer.

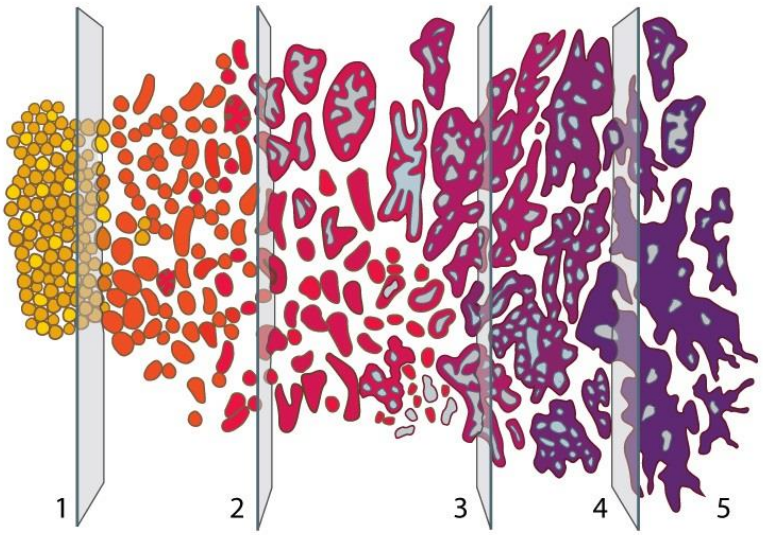

Figure 5: Gleason scoring system, from 1 (less aggressive) to 5 (most aggressive) (Adapted from Prostate Cancer Foundation of Australia).

The Tumor-Node-Metastasis (TNM) system is a globally accepted method to classify the extent of spread for cancer. It is based on three parameters: T, which defines the size of the primary tumor and its capacity to invade regional tissues, N, which describes near lymphatic ganglia that may be involved in the development of the disease, and M, which defines the possibility of metastasis, the propagation of tumor cells to other organs.

Analysing the TNM staging system (represented on Figure 6) it is possible to divide the pathology into three distinct groups: localized disease, where the tumor is confined to the prostate (T1 and T2); advanced, in which the disease evolves and extends to places out of the prostate capsule (T3), and even to adjacent structures like the bladder (T4); and metastatic, when the tumor invades lymph nodes (N) and forms distant metastasis in the bones and other organs, such as brain or lungs (M).

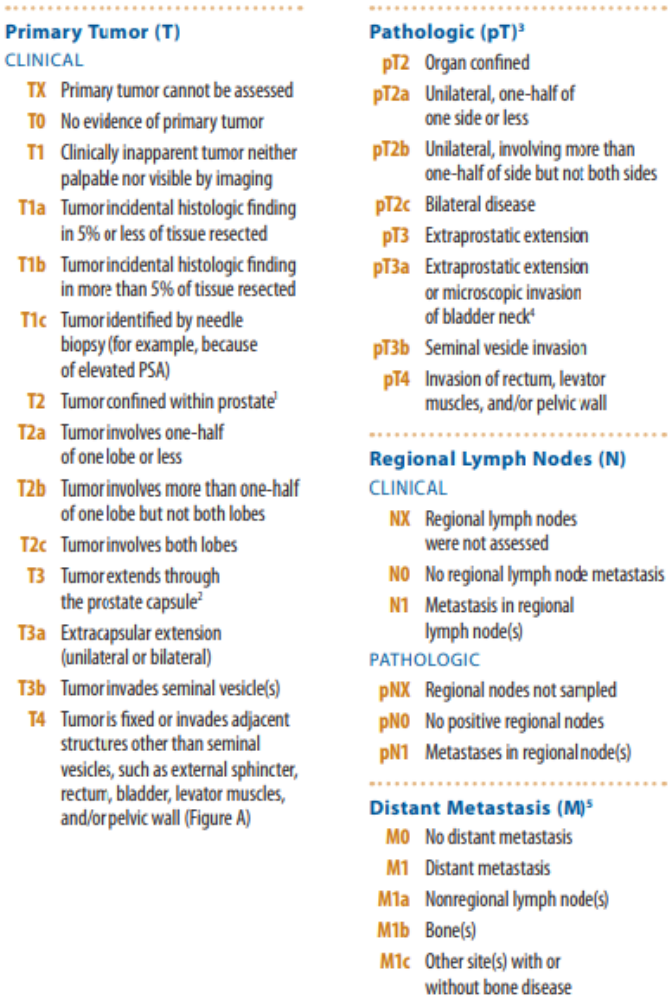

Primary Tumor (T)

CLINICAL

- TX Primary tumor cannot be assessed
- T0 No evidence of primary tumor
- T1 Clinically inapparent tumor neither palpable nor visible by imaging
- T1a Tumor incidental histologic finding in 5% or less of tissue resected
- T1b Tumor incidental histologic finding in more than 5% of tissue resected
- T1c Tumor identified by needle biopsy (for example, because of elevated PSA)
- T2 Tumor confined within prostate[1]
- T2a Tumor involves one-half of one lobe or less
- T2b Tumor involves more than one-half of one lobe but not both lobes
- T2c Tumor involves both lobes
- T3 Tumor extends through the prostate capsule[2]
- T3a Extracapsular extension (unilateral or bilateral)
- T3b Tumor invades seminal vesicle(s)
- T4 Tumor is fixed or invades adjacent structures other than seminal vesicles, such as external sphincter, rectum, bladder, levator muscles, and/or pelvic wall (Figure A)

Pathologic (pT)[3]

- pT2 Organ confined
- pT2a Unilateral, one-half of one side or less
- pT2b Unilateral, involving more than one-half of side but not both sides
- pT2c Bilateral disease
- pT3 Extraprostatic extension
- pT3a Extraprostatic extension or microscopic invasion of bladder neck[4]
- pT3b Seminal vesicle invasion
- pT4 Invasion of rectum, levator muscles, and/or pelvic wall

Regional Lymph Nodes (N)

CLINICAL

- NX Regional lymph nodes were not assessed
- N0 No regional lymph node metastasis
- N1 Metastasis in regional lymph node(s)

PATHOLOGIC

- pNX Regional nodes not sampled
- pN0 No positive regional nodes
- pN1 Metastases in regional node(s)

Distant Metastasis (M)[5]

- M0 No distant metastasis
- M1 Distant metastasis
- M1a Nonregional lymph node(s)
- M1b Bone(s)
- M1c Other site(s) with or without bone disease

Figure 6: TNM system for prostate cancer staging (Adapted from American Joint Committee on Cancer).

The information taken from grading (Gleason scoring) and from staging (TNM system) help specialists in decision-making about the best treatment approach for each patient.

Considering those parameters, in 1998 D'Amico and colleagues developed a staging system to stratify patients into three groups: low, intermediate or high-risk of recurrence after radical prostatectomy or radiotherapy. This system is based on the analysis of the clinical TNM staging system, the PSA level and the biopsy Gleason score (Boorjian et al., 2008).

In the D'Amico scoring, patients with T1c-T2a cancer, a PSA level of 10 ng/mL or less and a biopsy score of 6 or less are considered low-risk; those with T2b disease, PSA level of 10.1 to 20 ng/mL and Gleason score of 7 are of intermediate-risk; and patients with

clinical stage T2c, PSA level higher than 20 ng/mL and biopsy score from 8 to 10 are considered high-risk.

1.1.5. Treatment

Men diagnosed with localized disease usually have three primary treatment options: expectant management, surgery and radiation (Mottet et al., 2014).

In the expectant management, prostate cancer is monitored without resorting to definitive therapy, and consists in watchful waiting, with monitoring of disease progression. This option is valid for low-risk and active surveillance subjects, including a series of tests, especially PSA measurement, physical examination, prostate biopsies, or a combination of these to monitor the progression of the disease (Sathianathen et al., 2018).

For individuals with more significant disease, which possess a PSA level higher than 10 ng/mL and/or present palpable nodules on DRE, surgery and/or radiation continue to be the most used treatment approach in the clinical practice (Mottet et al., 2014).

The radical prostatectomy involves the removal of the prostate gland and the seminal vesicles. In what concerns to surgery, nowadays open radical prostatectomy has been largely replaced by laparoscopy and robotic radical prostatectomy, seeing as up to 40% of these are now robot-assisted (Shen and Abate-Shen, 2010). Clinical trials have supported the benefits of adjuvant local irradiation in avoiding local recurrences for those with more aggressive disease, and because of that, this course of treatment should be discussed with patients prior and after surgery.

The radiation treatment includes external beam radiotherapy or brachytherapy. External beam radiation therapy involves irradiations 5 days a week for 4 to 6 consecutive weeks with fractions of 1.8 to 2.0 Gy per day to total doses higher than 70 Gy (Daly et al., 2017). The main objective of the therapy with radiation is to deliver a curative dose of radiation to the prostate without damaging the proximal tissues, as it is the case of the bladder and the rectum. Brachytherapy involves the ultrasound guided placement of radioactive seeds or wires into the prostate tissue guided by ultrasound, which can be used alone or in combination with external beam radiotherapy (Gay and Michalski, 2018). There are two types of brachytherapy, low-dose rate and high-dose rate, being low-dose a permanent

implantation of radioactive seeds, whereas the high-dose is temporary and normally combined with external beam radiotherapy (Dunn and Kazer, 2011).

Cryotherapy is another treatment option that can be valid to men with high-risk disease if the prostatectomy is counter indicated. This intervention involves the freezing of the prostate gland. It induces damage on the cells by direct and indirect mechanisms at the time of the treatment and over time, dying the cells both by necrosis and apoptosis (Rodríguez et al., 2014). During cryotherapy, a cryoprobe is inserted in the prostate with ultrasound and the gland is frozen at a temperature of -100 to -200ºC during approximately 10 minutes (Dunn and Kazer, 2011).

1.2. Advanced Prostate Cancer and Androgen Dependence

Androgen dependence in prostate cancer was first discovered in 1941 by Charles Huggins, research that led him to win the 1966 Nobel Prize in Medicine and Physiology (Huggins and Hodges, 1941).

Androgens are synthesized in the testicles and the adrenal glands. Testosterone is the most abundant androgen, synthesized by the Leydig cells in the testis and converted in 5α-dihydrotestosterone (DHT) in the prostatic tissue by the activity of the 5α-reductase. DHT has higher affinity to the androgen receptors (AR) and connects to these, promoting prostatic cells differentiation processes. In addition, the adrenal glands produce some fewer common androgens, including androstenedione and dehydroepiandrosterone, which can be converted into testosterone (Tan et al., 2015).

The androgen receptors are members of the nuclear receptor superfamily. Circulating androgens are essential for the normal development of the prostate. However, they can also be involved in the process of carcinogenesis, because of their interactions with androgen receptors. The AR gene is localized in the X chromosome (Xq11-12), and it is composed by 8 exons that code the protein, which is about 11 kDa (Fujita and Nonomura, 2018a). In the prostate normal growth, the epithelial AR has a function of provide secretory proteins to the prostate, such as the PSA. However, in prostate cancer the AR has functions like PSA synthesis, regulation of lipid metabolism and promotion of cell growth (Shafi et al., 2013).

For men with advanced prostate cancer, the usual treatment courses are followed or replaced by androgen deprivation therapy (ADT), which consists in the removal of the testicular androgens by surgical (bilateral orchiectomy) or chemical castration. This therapy leads to prostate tumor regression (Harris et al., 2009).

The surgical bilateral orchiectomy consists in the removal of the testicles, reducing considerably the levels of testosterone. It has the advantage of being an efficient technique in the reduction of testosterone levels, but has the inconvenient of being an irreversible androgen depletion (Mottet et al., 2014).

At the time of prostate cancer's androgen dependence discovery, surgical castration was considered the gold standard for patients with advanced disease, but it was after largely replaced by methods of pharmacological castration, which allow intermittent androgen deprivation (Sathianathen et al., 2018). Pharmacological androgen deprivation is usually achieved by oral treatment with nonsteroidal antiandrogens like flutamide, which are used in combination with gonadotropin-releasing hormone (GnRH) analogues such as leuprolide and goserelin (Harris et al., 2009; Tan et al., 2015). This therapy has however been associated with toxicity, presenting secondary effects such as lowered mineral bone density, metabolic changes, and sexual and cognitive dysfunction (Kumar et al., 2005).

Although patients treated with ADT remain in long-term remission, this therapy is also associated with prostate cancer recurrence, taking the disease to a castration resistant status, which is currently still lethal (Harris et al., 2009).

1.3. Castration-resistant Prostate Cancer

For some years ADT has been accepted as standard treatment for advanced prostate cancer, however after a favourable initial response, malignant cells become resistant to the hormonal therapy after about 12 to 18 months of its beginning (Lassi and Dawson, 2009; Rodrigues et al., 2014).

Castration-resistant prostate cancer (CRPC) is defined as a disease that does not respond to ADT. Patients with prostate cancer can have secondary metastasis on sites like lungs, liver and pleura, but usually also have a tendency to form bone metastasis, with osteoblastic characteristics. This type of metastasis occur in up to 90% of patients with

CRPC, and cause symptoms such as pathological fractures, spinal cord compression and bone marrow failure, along with paraneoplastic effects like anaemia, weight loss, hypercoagulability and increased susceptibility to infection (Saad and Hotte, 2010).

Although CRPC is still a lethal disease, nowadays there are some therapeutic options to manage it (Figure 7). Currently, when patients have CRPC without metastases, they are usually treated with secondary hormonal therapy and screened for metastasis. In the case of metastasis with minor or inexistent symptoms the course of treatment includes abiraterone, enzalutamide or docetaxel. When there are major symptoms in metastatic castration-resistant prostate cancer (mCRPC), patients are treated either with docetaxel and/or Radium-223 (^{223}Ra). Besides ^{223}Ra, docetaxel may be combined with abiraterone, enzalutamide or cabazitaxel, with these being administered after docetaxel (Saad and Hotte, 2010; Sathianathen et al., 2018).

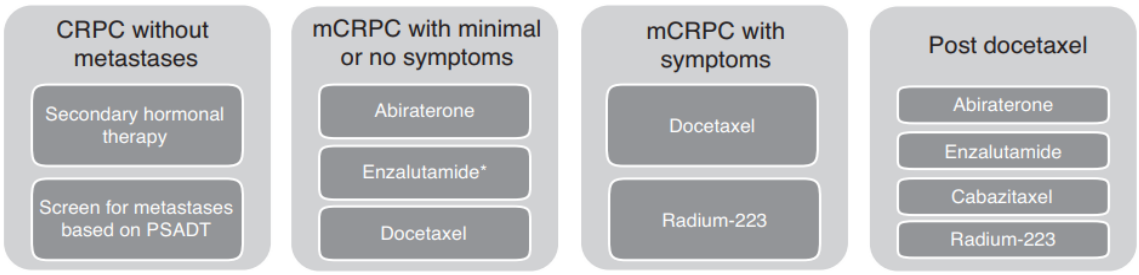

Figure 7: The 2015 CUA-CUOG Guidelines for the management of castration-resistant prostate cancer (CRPC) (Adapted from Saad et al., 2015).

Docetaxel is one of the chemotherapeutic options, since it was approved by the Food and Drug Administration (FDA) as first-line therapy for mCRPC in 2004. This drug leads cells to apoptosis through the inhibition of microtubule assembly and mitotic arrest (Ritch and Cookson, 2016).

The cabazitaxel is a semi-synthetic third generation taxane developed to break the resistance of cancer cells to docetaxel. Pre-clinical trials showed that this chemotherapeutic agent has a cytotoxic activity equal or superior to docetaxel, including in docetaxel-resistant cells. This drug was approved in 2010 by the FDA due to its benefits in the survival of docetaxel-resistant patients (Tsao et al., 2014).

The abiraterone acetate is a selective inhibitor of the androgen biosynthesis that blocks P450 c17 cytochrome inhibiting the conversion of cholesterol into testosterone and DHT. To prevent adrenal insufficiency, abiraterone acetate must always be administered with prednisone (Rodrigues et al., 2014).

The enzalutamide is an AR antagonist that is capable of blocking the connection of testosterone to the AR, preventing its migration in prostate cancer cells and inhibiting its connection to the DNA (Tran et al., 2009)

Sipuleucel-T was the first cancer vaccine to be available commercially. It is an autologous dendritic cell vaccine prepared from the patient's own antigen-presenting cells that have been exposed to prostate acid phosphatase (PAP). These activated dendritic cells induce then T-cell-mediated immunity when reinfused back into the patient, developing an immune response (Dowd et al., 2017; Sekhon et al., 2017). However, the vaccine high economic cost and clinical complexity can limit its use on the clinical practice (Rodrigues et al., 2014).

1.3.1. Radium-223 in the treatment of metastatic castration-resistant prostate cancer

A large percentage of patients (from 65% to 75%) with prostate cancer develop bone metastasis, which can lead to symptoms such as pain, hypercalcemia, lack of mobility and depression, factors that negatively affect the quality of life of these patients (Lewington, 2005).

Most patients with mCRPC develop bone metastasis, and it is a significant cause of mortality and morbidity on these patients, being associated with a very low survival rate (Ottewell et al., 2014). Visceral metastasis are less common in these patients, but they are still observed in approximately 10% of patients' diagnoses with mCRPC. The 5-year survival rate for men with mCRPC is 29% (Parker et al., 2018).

The bone metastisation occurs as a result of a multifaceted pathophysiological process between cancer and bone cells, which leads to cell invasion, migration and osteoblastic and osteoclastic stimulation. This process is moderated by cytokines, hormones and tumor derived growth factors (Roato, 2013).

Some radiopharmaceuticals can be used for palliative treatment related to bone metastasis. One of the great challenges associated with these radiopharmaceuticals is the delivery of an adequate dose of radiation to the bone lesion, minimizing the dose to healthy bone sites and adjacent tissues, while keeping the looked-for therapeutic effect(Chakraborty et al., 2008; Liberal et al., 2017).

There are essentially three types of radioactive particles that are of interest to tumor targeted radiotherapy, the beta minus particles (β^-), the alpha particles (α) and the Auger electrons. The β^- particles usually have an irradiating range of several millimetres in the tissue, fact that can lead to the irradiation of tumor adjacent healthy tissues. On the other side, α particles typically have a penetrating range of less than 100 μm, whereas Auger electrons are low-energy electrons with very low penetration ranges, in the order of nanometres to micrometres (Liberal et al., 2017).

Xofigo® (Bayer, Germany) is a solution of ^{223}Ra dichloride. It was approved in 2013 by the EMA (European Medicines Agency) and the FDA (Marques et al. 2018; EMA 2014). It is an alpha particle emitter that has been showing great promise in the palliative treatment of bone metastases derived from prostate cancer, since it has the advantage of possessing a very low penetration range in the tissue, typical characteristic of α particles. When it is produced it has a specific activity of 1100 kBq/mL. In clinical trials, ^{223}Ra has been showing an overall improvement in survival rate of patients, with minor secondary effects due to its localized penetration (it affects only from 2 to 10 cells in the tissue) (Harrison et al., 2013). Previous studies showed that ^{223}Ra induces a major number of lesions in DNA, provoking a high number of double-strand breaks and a low probability of those breaks being fixed by the repair processes (Liberal et al., 2017). It mimics calcium, is absorbed in areas with high osteoblastic activity and rapid bone turnover and connects to the bone matrix through the bone hydroxyapatite (Figure 8) (Fizazi et al., 2009; Odo et al., 2017).

The range of ^{223}Ra α particles is <100 μm, which allows an elevated effect on tumor cells, while minimizing the risk of damage in the bone marrow and other healthy tissues. The most common side effects of ^{223}Ra are diarrhoea, nauseas, vomit and thrombocytopenia (Parker et al., 2013).

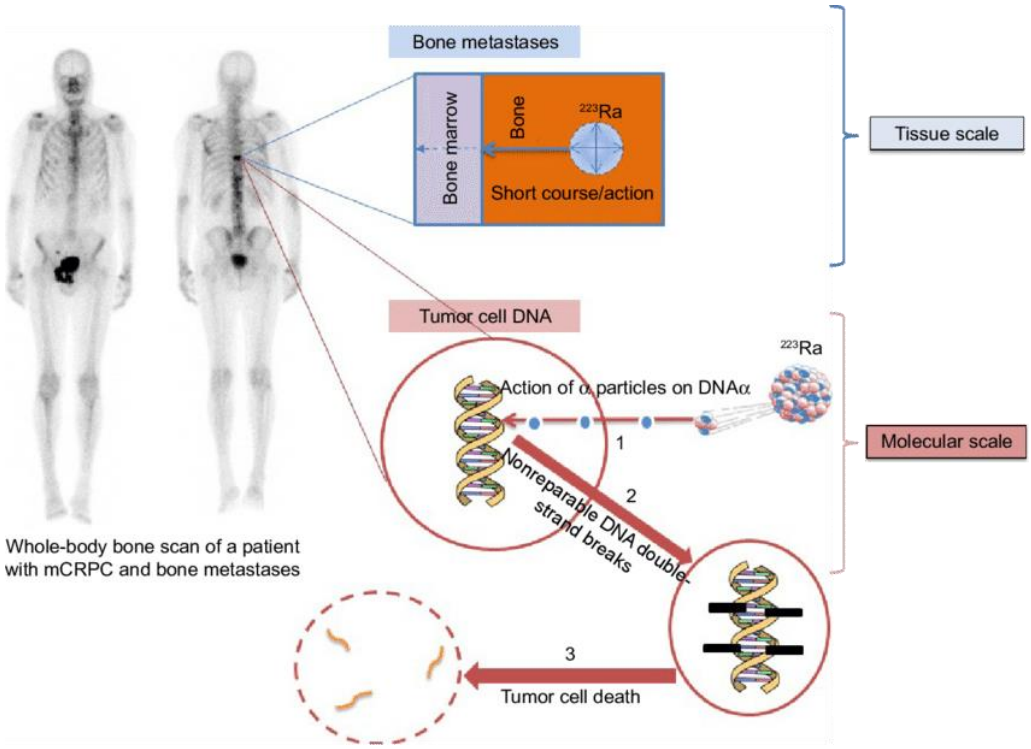

Figure 8: Mechanism of action of Ra-223 on a tissue and molecular scale (Adapted from Deshayes et al., 2017).

These properties are of great benefit when compared with beta particle emitters such as Samarium-153 and Strontium-89, because it presents a greater index of breaks in the DNA double chain, with lesser haematological toxicity for the patients (Jacene et al., 2018). The high linear energy transfer (LET) of the α particles and the limited ability of cells to repair the DNA damage caused by α radiation explain its cytotoxicity and relative biological effectiveness (Lassmann and Eberlein, 2018).

The ionizing radiation can induce direct or indirect effects on cells. The α particles are usually associated with direct effects, due to the fact that they have high energy, enough to extract electrons from atoms or molecules. Since these particles are heavy and slow, they cause direct cellular damage in biomolecules such as DNA, resulting in cell death. In terms of indirect effects, these may occur mainly due to oxidative stress originating from radical species as a result of water radiolysis. The cell is composed of 80% of water, being its major component and, as a result, extremely reactive free radicals are produced, such as oxygen reactive species (ROS) (Mendes et al., 2015; Marques, 2016).

The α particles have positive charge and they are constituted by two protons and two neutrons, whose mass and charge are equal to a helium nucleus. In terms of clinical application, this structure confers them a superficial penetrating range that is capable of getting to the cortical region of the bone, where usually are located the metastases of prostate cancer. The LET of these particles is in the range of 80-100 keV/µm, which means that it is a type of radiation with a high LET. Due to this fact, α particles deposit great quantities of energy in short distances, avoiding damage to adjacent normal tissues and potentiating the tumor cells' death (Sgouros, 2008; Marques et al., 2018).

^{223}Ra has a half-life of 11.4 days and decays until the stable Lead-207 (^{207}Pb), generating four α particles. During its decay, the release of α particles constitutes 95.3% of its total decay energy, whereas the β emission comprehends 3.6% and γ 1.1% (Marques et al., 2018). The decay chain of ^{223}Ra is represented in Figure 9.

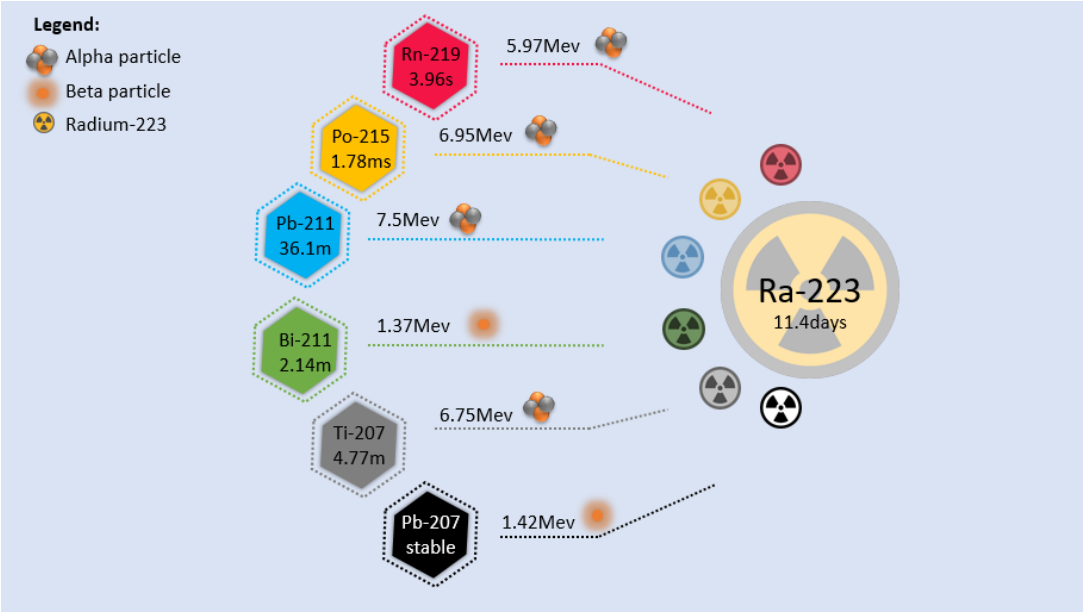

Figure 9: Decay chain of Radium-223. (Taken from Marques et al., 2018).

The approved dose regimen of ^{223}Ra is an activity of 55 kBq/kg administered in six intravenous injections at 4-weekly intervals, administered by slow intravenous injection (generally for one minute). It was the first targeted alpha therapy to be approved by the FDA that has proven effects on the raise of the overall survival rates on patients with mCRPC,

and its clinical use has been raising ever since (Deshayes et al., 2017; Du et al., 2017; Marques et al., 2018).

The half-life of ^{223}Ra is optimal for clinical use, because it allows enough time for its preparation, distribution and administration. After injected in the patient it is rapidly eliminated from blood flow, and it is known that the primary excretion pathway of the radiopharmaceutical is through the small intestine and faeces (Buroni et al. 2016).

The fact that alpha particles have a very small penetration range and are easily shielded makes the manipulation of this radiopharmaceutical relatively simple, as it can be administered by a normal syringe, without complex proceedings of shielding, monitorization or radiation protection. The elimination of the radioactive residues of the ^{223}Ra is meant to be done 4 months after the administration on the patients, and they are discarded as normal radioactive clinical trash (Parker et al., 2018).

^{223}Ra is indicated for patients with mCRPC with symptomatic bone metastases and no known visceral metastases. Studies have shown that the treatment with ^{223}Ra should be considered earlier in this type of patients to raise its efficacy and improve their quality of life (Saad and Hotte, 2010).

This radiopharmaceutical was approved based on the results of the phase-3 international clinical trial Alpharadin in Symptomatic Prostate Cancer (ALSYMPCA), performed on patients with symptomatic mCRPC and bearers of bone metastases. This trial showed that ^{223}Ra combined with the best standard treatment allowed to raise the overall survival rate of these patients when compared with a placebo, and also led to a decrease of the risk of symptomatic skeletal events (Parker et al., 2013, 2018).

More recently in 2019, a study funded by Bayer named ERA 223 studied the treatment of patients with mCRPC with ^{223}Ra in conjugation with abiraterone plus prednisone, given that both these courses of treatment had improved overall patient survival separately. In spite of this, the use of the combination did not show improvements of symptomatic skeletal events in patients with mCRPC and bone metastases, and was even associated with an increased number of bone fractures (Smith et al., 2019).

Besides being approved for the treatment of mCRPC, ^{223}Ra has been studied as a therapy hypothesis for osteosarcoma, being present in a preliminary Phase I dose escalation

clinical trial with 18 patients, where it showed promise. However, the recommended dose proposed for Phase II trials on patients with osteosarcoma is 100 kBq/kg monthly, which is twice the dose approved for the treatment of prostate cancer (Kairemo et al., 2019; Subbiah et al., 2019).

1.4. Cancer Microenvironment and 3D Cultures

The evaluation and approval of cancer therapeutics involve a series of steps which include *in vitro* and *in vivo* studies before passing to clinical trial phases. However, to rightfully assess an optimal dose of therapeutics, two-dimensional (2D) cell cultures are not enough in terms of tumor microenvironment complexity mimicry (Jaganathan et al., 2014). With this in mind, in terms of complexity, three-dimensional (3D) cultures can be a major asset to close the gap between 2D cell culture studies and animal models (Cukierman et al., 2001).

Nowadays, the approval rates for new cancer drugs are less than 5%, although very significant efforts are being made in the cancer research and development of novel neoplastic drugs (Sant and Johnston, 2017). A strategy that could be very useful to significantly raise the success rate for the discovery and subsequent transition from *in vitro* studies to clinical trials of new cancer treatments could be the approximation of cellular models to animal models and patient tumors, in terms of complexity and environment (Carvajal et al. 2012).

A solid tumor is not only composed by tumor cells, but also by stromal cells and extracellular matrix (ECM) components that cohabit in a tumoral three-dimensional microenvironment where cellular function and behaviour are mediated by cell-cell, cell-ECM interactions and local gradients of nutrients, growth factors and oxygen (Friedrich et al., 2009; Sant and Johnston, 2017). The tumor microenvironment is a framework of connective tissue with stromal cells that interact both structurally and functionally with the cancer cells, and it includes fibroblasts, endothelial cells and various types of immune system cells (Eger and Mikulits, 2005).

Most of cancer-caused deaths are not triggered by the primary tumor, but by secondary tumors formed through the complex and still poorly-understood process of metastasis (Figure 10) (Sleeboom et al., 2018).

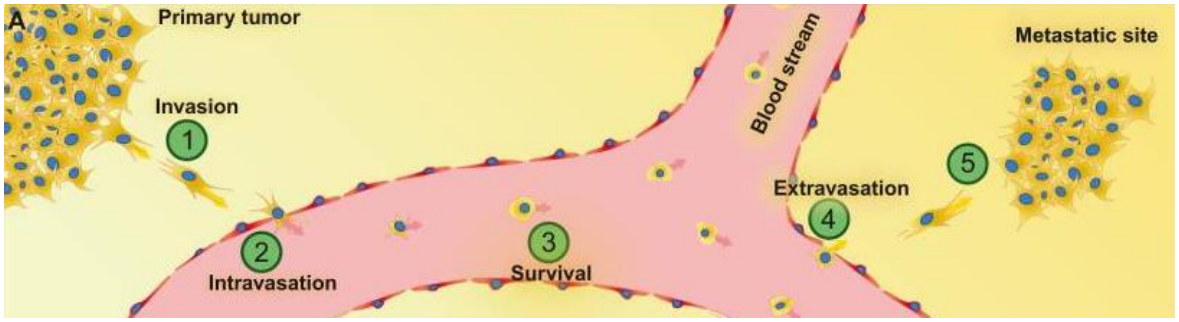

Figure 10: The 5 steps of metastasis: invasion, intravasation, survival, extravasation and secondary tumor development (Adapted from Sleeboom et al., 2018).

The "leakage" of cancer cells from the primary tumor is mostly associated with epithelial dedifferentiation with the loss of intracellular adhesion and a profile of raised invasive potential (Friedl and Wolf, 2003; Eger and Mikulits, 2005).

The process of the metastatic cascade is related with the infiltration of tumor cells in tissues adjacent to the primary tumor, transendothelial migration of cancer cells to the blood flow (process known as intravasation), the survival of the cells in the blood stream, extravasation into other tissues from the circulatory system and subsequent proliferation into other organs leading to their colonization (Eger and Mikulits, 2005; van Zijl et al., 2011; Sleeboom et al., 2018).

One of the biggest challenges on treating any type of cancer is the complexity and heterogeneity of tumors on each individual, that can lead to resistance to therapy (Hoarau-Véchot et al., 2018).

Currently, most of the *in vitro* studies are still made in monolayer, but since the 90's there has been a huge increase in the number of publications on 3D cell culture methods and experiments, leading to a maximum number of 1363 articles on the theme in 2018, according to PubMed, using as research words "three dimensional cell culture". These 3D cell culture models have been establishing themselves as a halfway in complexity between monolayer and animal models (Figure 11), due to their closer approximation on tumor biology characteristics when compared to the traditional monolayer cultures (Caicedo-Carvajal et al. 2012).

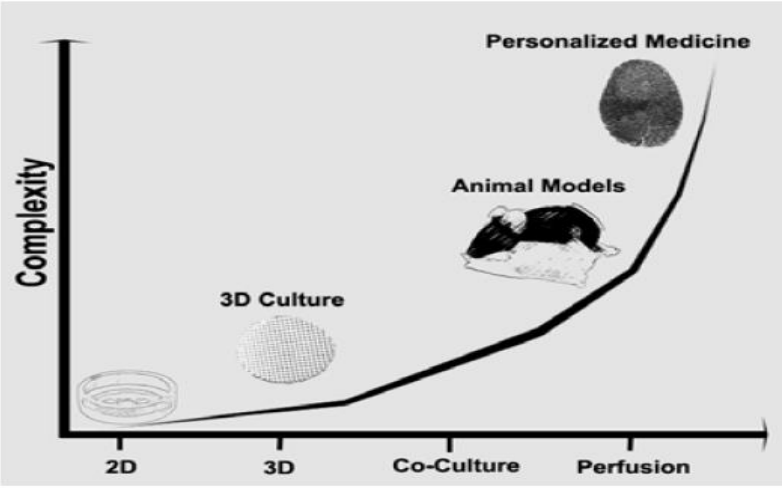

Figure 11: Scheme representing complexity versus technique (*in vitro* and *in vivo*) (Adapted from Caicedo-Carvajal et al., 2012).

Taking into account the high cancer incidence and mortality, the limitations present in diagnosis and treatment and the raised use of 3D cell culture models in cancer research, it is very important to study the options for modelling cancer cells in 3D, as well as the advantages, boundaries, and applications in research and clinical practice (Hoarau-Véchot et al., 2018; Kapałczyńska et al., 2018). Thus, it is clear that 3D cell culture models play an important role in the growing and promising field of personalized medicine.

Solid cancers are heterogenic tumoral masses with different environments from the center to the surrounding tissue. At cellular level, different micro environmental conditions influence the acquisition of an invasive potential and uncontrolled division of cells. This process is also accompanied by the creation of a stroma, which includes an augmented vascularization. Overall, the 2D approach does not mime the in situ environment of tumours or normal tissues, is not representative of 3D cell morphology and can distort cellular interactions (Cukierman et al., 2001). One of the biggest inconvenient of in vitro 2D cultures is the failure in maintaining the phenotype and complexity of the primary tumor over time (Porter et al., 2014).

3D cell culture models range from simple spheroids of a cancer cell line to models that comprehend multiple cell lines or primary cultures derived from patients. They are used to represent a closer replica of the tumoral microenvironment, and provide a compromise

between the monolayer and the complex and extended process of growing human tumors in xenogeneic animal models (Nyga et al., 2011).

Three-dimensional studies have been demonstrating different cell morphology when compared with 2D, showing the important role these techniques can have on cancer research. The models explored so far have showed promising results, including aggregation and clustering of cancer cells, migration and proliferation, releasing of angiogenic factors and formation of hypoxic centres inside tumor spheroids. They are also useful to test the efficacy and mechanisms of novel and existing drugs.

Nowadays there are already some options on modelling tumors in three-dimensions, which can be classified into 3 major groups: the 3D scaffold-based cultures, the 3D non-scaffold-based cultures and the inserts. They all can make viable examples of cancer spheroids and have advantages and disadvantages.

Cancer spheroids can be composed exclusively by cancer cells, which are designed homotypic spheroids, or by cancer cells cultivated in co-culture with other types of normal cells, such as fibroblasts or epithelial cells, which are called heterotypic spheroids. 3D cultures, as all cells grow in close contact, are a better fit reproduction of the physical communications and the signalling pathways observed in solid tumors (Chandrasekaran et al., 2012; Costa et al., 2016).

Like in solid tumors, the internal structure of spheroids is composed by different cell layers. In the literature, these are usually divided into 3 principal layers: the external layer, composed by cells presenting a high proliferation rate, the middle layer, which is usually essentially formed by senescent cells blocked in the cell cycle, and the core, which contains necrotic cells (Figure 12).

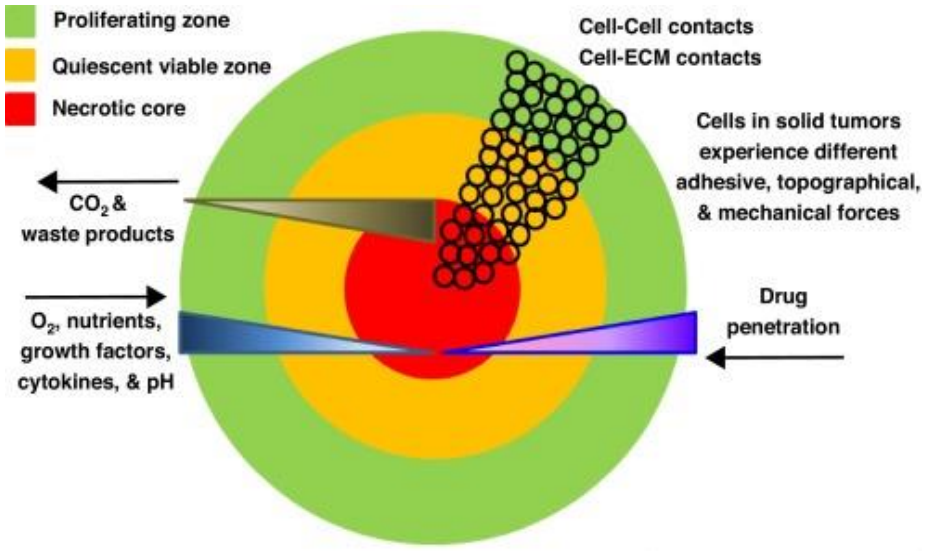

Figure 12: Spheroid tumor model and principal characteristics (Adapted from Sant and Johnston, 2017).

The higher proliferation rate of the cells in the periphery of the spheroid is explained by the easier access to oxygen, metabolites, signalling molecules and nutrients in the culture medium, whereas the cells in the more internal layers remain in a necrotic or senescent state due to the lower contact with nutrients and oxygen, which can provoke hypoxia in the cells (Costa et al., 2016; Kapałczyńska et al., 2018).

CHAPTER 2 - OBJECTIVES

Taking into account the fact that prostate cancer is one of the highest incident and mortal cancers worldwide and that metastatic castration-resistant prostate cancer still has very poor prognosis for patients overall, there is a need for the study of new hypothesis of treatment. The ^{223}Ra is a radiopharmaceutical approved by the FDA and the EMA that is suited for patients with mCRPC with bone metastasis, whose mechanism of action in the cancer and normal tissue cells is not yet fully disclosed.

Thus, the objectives of this work passed by studying prostate cancer's metastatic microenvironment using a cell line from a bone metastatic niche (PC3), implementing, optimizing and characterizing a 3D cell culture model with this cell line and then evaluate the model's response to ^{223}Ra therapy and its effects through cellular and molecular biology techniques.

CHAPTER 3 – MATHERIAL AND METHODS

3.1. Cell Culture

In order to make the *in vitro* studies two prostate cancer cell lines were used, LnCap and PC3. Both the cell lines were acquired from the American Type Culture Collection (ATCC).

PC3 (ATCC® CRL-1435™) is a prostate cancer cell line resulting from a bone metastasis derived of a 62 year old Caucasian male that was diagnosed with a Grade IV prostate adenocarcinoma in 1979. The LnCap (ATCC® CRL-1740™) cell line was obtained in 1977 from a 50 year old Caucasian male and it is derived from the left supraclavicular lymph node. Besides the origin of the cells, these two cell lines also differ on their dependence on hormones, growth rate and invasiveness, being that the PC3 cell line is not hormone dependent, its proliferation does not depend on the presence of androgens, and it has a high growth rate and metastatic potential, whereas the LnCap have a low growth rate, small metastatic potential, express hormone receptors, PSA, and its growth is inhibited by the lowering of androgens, fact that indicates a hormone dependency (Domińska et al., 2016).

After the reception of the two lines, they were defrosted and maintained in a Binder incubator (Binder, Germany), with a humid atmosphere at 37ºC, 95% air and 5% carbon dioxide (CO2), according to the ATCC guidelines.

The culture medium Roswell Park Memorial Institute (RPMI) was used to cultivate both prostate cancer cell lines. This medium was supplemented with 10% fetal bovine serum (FBS) (Sigma F7524), 100µM of sodium pyruvate (Gibco 11360) and antibiotic (Sigma A5955) to make 1% concentration.

Both cell lines grow in adherent monolayer, and to prepare the 3D structures we needed the cells in suspension, so it was needed to detach them from the flasks. With that purpose, it was removed the culture medium and the cells were washed with phosphate buffered saline (PBS), with a 7.4 pH. The PBS was then discarded, and it was added 2 mL of Tryple^{TM} Express (Gibco, 12605-028). After 5 minutes in the incubator for the compound to act faster, the effect of the Tryple was inhibited using 5 mL of fresh medium. Later, after obtaining the cell suspension, it was determined the cell concentration with the trypan blue exclusion method. This method is essentially based on the fact that viable cells maintain

their cell membrane intact (brilliant on the microscope), whereas dead cells are permeable to the trypan blue, possessing then a blue cytoplasm.

To perform this method, it were used 20 µL of cell suspension and 20 µL of trypan blue 0.02%, and the cell concentration was determined by counting the cells (both alive and dead) of the 4 quadrants in a Neubauer chamber, using an inverted optic microscope with a 100x magnification. The formula used to calculate cell concentration was the following:

$$[\text{Cell}]\ (\text{cells/mL}) = \text{Alive cells (average of the 4 quadrants)} * 2 * 10\,000 \qquad \textbf{Equation 1}$$

3.2. Establishment of Prostate Cancer 3D Cell Cultures

One of the principal objectives of this work passed by obtaining 3D cell cultures of prostate cancer cells. To achieve that, it was used a protocol of an adaptation of the magnetic levitation method (MLM), which was developed by Glauco Souza and colleagues, and published in 2010 (Souza et al., 2010; Becker and Souza, 2013; Haisler et al., 2013). This protocol is based on the incorporation of a magnetic nanoparticle by the cells, which allows them to stay in suspension on the culture medium and aggregate through the action of an external magnetic field.

To start the protocol, it is mandatory to detach the cells from the flasks using Tryple. The cells were then counted by the trypan blue exclusion method and were plated on small Petri dishes, using a concentration of 2 x 10^6 cells per millilitre, leaving them overnight so that they have time to attach to the dishes. The next day, to each Petri dish, it was added 60 µL of NanoShuttleTM (Figure 13, biocompatible magnetic iron oxide-gold-nanoparticle, ~50nm), which attaches electrostatically to the cell plasma membrane, and they were left in the incubator overnight so that the cells can incorporate the nanoparticle.

Figure 13: Magnetic nanoparticle used in the magnetic levitation method.

After that incubation time, the cells were detached from the dishes, counted once more by the trypan blue exclusion method and plated in a concentration of 2 x 10^5 cells in 250 µL of fresh medium per well in low-attachment 24-well plates, to avoid cell's attachment to the bottom of the plates, as they are adherent cells and it is required that they stay in suspension to make 3D culture spheroids. In the end, it is placed a magnetic levitation plate called levitating drive (Figure 14A) over the multi-well, which is composed by magnets that stay over each well in a way that the cells which incorporated the nanoparticle are attracted by the magnet, stay in suspension and remain levitating in the medium, interacting with each other and aggregating, forming that way a 3D spheroid (Figure 14B).

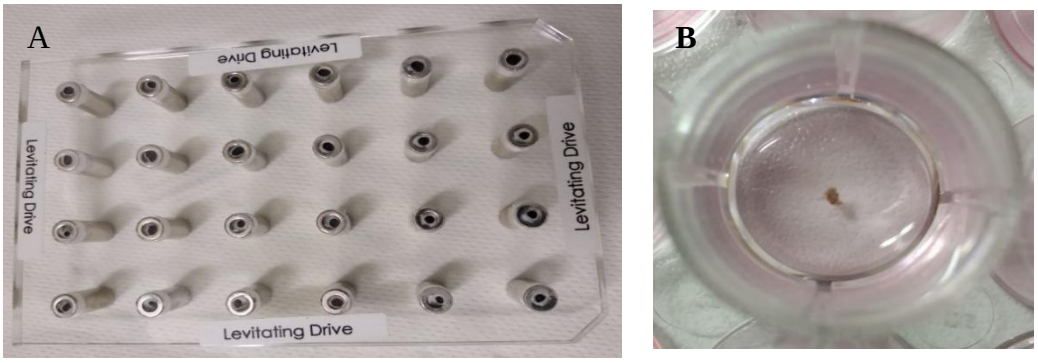

Figure 14: Levitating drive used to attract the cells with magnets after the inoculation with the magnetic nanoparticle (A) and spheroid formed after the application of the MLM (B).

The 3D culture has an average duration of 7 days since the day it is established. After that period, it can be observed some disaggregation due to the fact that the cells start to disincorporate the magnetic nanoparticle (Haisler et al., 2013).

In the case it is needed to change the spheroid culture medium, the low attachment plate is placed over the concentrating drive (Figure 15) so that the cells stay attached to the bottom of the plate. Posteriorly, the old medium is taken out and new medium is added.

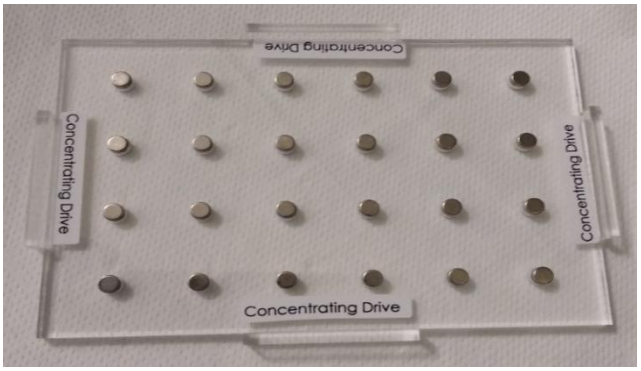

Figure 15: Concentrating drive, used to change the medium of the 3D cultures.

To perform some experiments, it was required that the spheroid would be taken out of the well intact. In order to achieve that, it was used a MagPen, a small plastic "pen" with a magnet inside. Once inside the well, the spheroid binds to the pen and it can then be transferred to other plate, or for example a microscope slide, just by taking out the magnet inside the pen.

3.3. Irradiation of Prostate Cancer 3D spheroids with Radium-223

After seeding 2 x 10^5 cells per well in low-attachment 24-well plates and applying the levitating drive, the spheroids were left to aggregate and grow for 48 hours, and then irradiated.

To perform each assay, the spheroids were submitted to internal irradiation by exposure to Radium-223, with the addition of a constant activity A_0. Previously doses and respective times were calculated (Table 1), through Equation 2:

$$D = \frac{A_0}{\ln 2 M} \sum_i \alpha_i \, T_i \left[1 - e^{-\frac{\ln 2}{T_i} t}\right] \bar{E}_i \qquad \textbf{Equation 2}$$

where D corresponds to absorbed dose (Gy), A_0 to the initial activity of the radioactive source (Bq), α_i to the decay energy fraction, T_i to the period of semi disintegration of the i portion in the decay chain (s), t to the irradiation time (s), $\bar{E}_i$ to the medium energy per disintegration of the i portion in the decay chain (eV) and M to the mass of the sample subjected to irradiation (kg). The values of α_i, T_i and $\bar{E}_i$ represent listed parameters that are specific to the type of radiation used.

The irradiation procedure involved adding an activity of 0.3 µCi to the 3D prostate cancer spheroids, which are in suspension in a constant volume of medium (250 µL) for an irradiation period t, determined previously by Equation 1, to obtain a defined absorbed dose D. The values of dose and its respective irradiation time periods are presented on Table 1.

Table 1: Doses, initial activities and times used in the irradiation with Radium-223.

Dose (mGy)	A_0 (µCi)	Time (min)
1	0.3	0.85
4	0.3	4.50
10	0.3	15.05
15	0.3	25.00
20	0.3	35.00
30	0.3	55.00

After the respective time of irradiation, the old medium was suctioned with the help of the concentrating drive to avoid losing the spheroids, replaced with fresh one and the spheroids were kept in the incubator for 48 hours, until they were taken out for the experiments. All the irradiation protocols were made accordingly to the norms of radioprotection.

3.4. Analysis of Protein Content by the Sulforhodamine B (SRB) assay

The SRB assay has been broadly used to evaluate cell proliferation and cytotoxicity of compounds. This method uses a fluorescent dye called sulforhodamine B, which binds to proteins under acidic conditions and can be posteriorly extracted under basic environment, so the amount of dye can be extrapolated to measure protein content and indirectly cell proliferation (Vichai and Kirtikara, 2006; Orellana and Kasinski, 2016).

The protocol was started by destroying the spheroids with the help of a micropipette and centrifuging them in a plate centrifuge at 300 G for 5 minutes. After that, the medium was discarded, and cells were fixed by adding 100 µL of a 96% TCA solution, leaving it to act for 1 hour. Posteriorly, TCA solution was discarded, and it was added to the fixed cells 200 µL per well of sulforhodamine B, and incubated for 2 hours away from the light. Afterwards, the SRB was taken out with the help of a micropipette, the plate was carefully washed in order to remove the excessive unbound dye and dried at room temperature for 10 minutes. Once it was completely dry, it was added 200 µL of Tris-NAOH (pH=10) and the plate was left agitating for 15 minutes until the dye was totally dissolved. Next, the content

of the wells was transferred to 96-well plates and the absorbance read at 540 nm, with a reference filter of 690 nm, in an ELISA spectrophotometer (Biotek *Synergy HT*, USA). Results are expressed by the percentage of inhibition of irradiated cells' proliferation in comparison to the controls, normalized to 100%.

3.5. Cell Proliferation Analysis by Alamar Blue Assay

Alamar blue (Sigma, USA) is an oxidation-reduction probe used to evaluate cell proliferation that monitors the reducing environment of the cell. This can be done mostly due to the fact that metabolically active and proliferating cells present a reduced environment, whereas the inhibition of cell growth leads to an oxidized cell environment. The active ingredient in the compound is the resazurin, which is stable in culture medium, non-toxic to cells and permeable through cell membranes. This probe presents two forms, a non-fluorescent blue form that is oxidized and becomes fluorescent and pink resorufin when it is reduced (Figure 16). This characteristic of the probe gives this assay the advantage of being able to be measured quantitatively in colorimetric and/or fluorometric readings (Rampersad, 2012; Eilenberger et al., 2018).

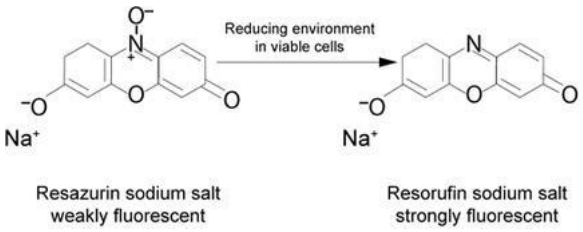

Figure 16: Alamar blue reaction in the cellular environment (Adapted from Bionity.com).

To perform this experiment, the PC3 spheroids were plated as explained before (2 x 105 cells in 250 µL of medium) and left to grow for 48 hours, then irradiated with the radiopharmaceutical Ra-223 as referred above. The analysis of the therapeutic effects of Ra-223 was made 48 hours after the irradiation. To do so, it was added 25 µL of alamar blue (1mg/mL) to each well, in a volume ratio of 1:10, incubating it for 1 hour and 15 minutes in the dark. The results of the assay were calculated using Equation 3, and are expressed according to the percentage of proliferation inhibition of irradiated cells in comparison to the control cells, which were normalized to 100%, after reading in an ELISA spectrophotometer at 570 and 600 nm (Biotek Synergy HT, USA).

$$\%\ \text{proliferation} = \frac{(\varepsilon OX)\lambda 2\ A2\lambda 1 - (\varepsilon OX)\lambda 1\ A\lambda 2\ \ (\text{irradiated cells})}{(\varepsilon OX)\lambda 2\ A^0\lambda 1 - (\varepsilon OX)\lambda 1\ A^0\lambda 2\ \ (\text{control cells})} \quad \textbf{Equation 3}$$

where (εOX) corresponds to the molar extinction coefficient of the oxidized form of the alamar blue (which is a tabled value), A to the absorbance of the irradiated wells, A^0 to the absorbance of the control wells, and λ1 and λ2 to 570 nm and 600 nm respectively, the absorbances measured in the spectrophotometer.

3.6. Cell Metabolism Evaluation by MTT Assay

The MTT assay was used to analyse cell metabolism in 2D with 3 different conditions, control, control+NanoShuttle and control+magnet, to check if the nanoparticle and the magnetic field generated by the magnet have any nefarious effects on the metabolism of the cells. These studies were made at 5 time points, 1, 2, 4, 6 and 8 days after plating.

To evaluate cell metabolism, the culture medium was discarded from the plates and the wells were washed with 500 µL of PBS (Sigma, USA) each. It was added 300 µL of a MTT solution (0.5 mg/mL) diluted in PBS at 7.4 pH and proceeded to an incubation in the dark, for 5 hours. After incubation, in order to dissolve the formazan crystals, it was added 300 µL of a 0.04M of acid isopropanol and the plates were agitated for 20 minutes. After the solubilization of the crystals, 200 µL of the content of each well was transferred to a 96 multi-well, measuring posteriorly the absorbance in an ELISA spectrophotometer (Biotek Synergy HT, USA), in a wavelength of 570 nm and a reference wavelength of 620 nm.

3.7. Morphology Studies by the May-Grünwald-Giemsa Staining

The May-Grünwald Giemsa stain is composed by a mix of two neutral stains, a May-Grünwald stain (0.25 g/mL) composed by eosin and methylene blue, and a Giemsa stain (0.25 g/mL) composed by eosin and azure of methylene. It is widely used in medicine and biomedical investigation to characterize cell populations and distinguish certain aspects of cell morphology (Sabattini et al., 2018).

To perform the staining, the spheroids were destroyed, their content was taken out the of the wells into 12 mL falcon tubes and these were centrifuged at 1300 xG for 5 minutes. After the centrifugation, the medium was discarded, as the pellet should contain both alive

and dead cells, and these cells were resuspended in a small quantity of FBS. After resuspending well with a micropipette, it was put a drop of cell suspension on a glass slide and it was performed a smear. The smears were left to dry at room temperature away from the light for 3 hours and after that fixed on 96% ethanol. After fixing, the slides were once again left away from the light until they dried, and the fixed smears were then stained in May-Grünwald diluted in an equal volume of distilled water for 5 minutes. Subsequently, the slides were put without washing into Giemsa stain diluted in a reason of 1:10 with distilled water, for 30 minutes. After staining, the slides were washed in tepid water and left to dry at room temperature. The slides were visualized and evaluated on an optical microscope Axioskop 2 (Zeiss, Munich, Germany) equipped with an Axiocam 1Cc3 camera (Zeiss, Munich, Germany), and then pictures were taken and analysed using AxioVision software (Zeiss, Munich, Germany) for Windows. The staining was performed on control and irradiated slides (10 mGy), both with cells from monolayer and 3D spheroids.

3.8. Histological Staining

Histological staining of spheroids or tissues fixed in paraformaldehyde (PFA) is a set of technical proceedings that allow for the analysis of a determined tissue at the optic microscope and subsequent visualization and evaluation of cellular structures (Bancroft and Gamble, 2008).

3.8.1. Haematoxylin and Eosin (H & E)

The spheroids were transferred to a slide with the help of the MagPen, fixed in a 4% solution of PFA for 3 hours and then washed 3 times for 15 minutes with PBS. Posteriorly, they were hydrated with a 70% ethanol solution, submerged in a hematoxylin solution (Ventana Medical Systems, USA) for 3 minutes and washed with tap water. They were then also submerged in an eosin solution (Ventana Medical Systems, USA) for 3 minutes and washed again with tap water and distilled water. After that, they were left to dry and mounted with QuickD synthetic mounting medium (Klinipath, Netherlands) to posterior observation in the optic microscope Olympus U-D30 (Olympus, Japan).

3.8.2. Toluidine Blue

For the toluidine blue coloration, the fixation process of the spheroids was the same as described before for the H & E staining. After fixating and washing with PBS, the spheroids were stained with a 0.4% toluidine blue solution (Ventana Medical Systems, USA) for 2 minutes. After staining, the slides were washed with distilled water to remove the excess dye and dried at room temperature. Subsequently, the slides were mounted with QuickD synthetic mounting medium (Klinipath, Netherlands) and observed in the optic microscope Olympus U-D30 (Olympus, Japan).

3.9. Protein Markers Presence by Immunocytochemistry

Immunocytochemistry was performed to compare and characterize protein expression between non-irradiated cells cultured in monolayer (2D) and in spheroids (3D).

The antigenic detection was made with an indirect system of biotin-free multimers conjugated with peroxidase, in a proceeding with the temperature set to 36ºC.

The inhibition of the endogenous peroxidase was made with a 3% H2O2 solution diluted in PBS called OptiView Peroxidase Inhibitor for 10 minutes, followed by the detection of the different primary antibodies with a cocktail of secondary goat antibodies IgG e IgM anti-mouse and goat IgM anti-rabbit (OptiView HQ Universal Linker, Ventana Medical Systems, USA), conjugated with a non-endogenous haptene, 3-hydroxy-2-quinoxaline (HQ), for 12 minutes. After washing the slides with PBS, it was dispensed the indirect detection system of multimer OptiView DAB IHC Detection Kit (Ventana Medical Systems, USA), free of biotin and conjugated with peroxidase for 8 minutes. Subsequently, the slides were mounted and observed at the Olympus U-D30 (Olympus, Japan) optic microscope, equipped with a camera Olympus SC30 (Olympus, Japan). The antibodies used and their respective characteristics can be observed in Table 2.

Table 2: Antibodies used in the immunocytochemistry studies and respective characteristics (clone, incubation time, dilution and provider).

Antibody	Clone	Incubation Time (min)	Dilution	Provider
KI-67	SP6	20	1:1000	Zytomed Systems, Berlin, Germany
Caspase 3	pAb	28	1:100	Bio-rad, California, USA
P16	E6H4	4	Ready to use	Ventana Medical Systems, Arizona, EUA
P53	DO-7	24	Ready to use	Ventana Medical Systems, Arizona, EUA
Vimentin	V9	4	Ready to use	Ventana Medical Systems, Arizona, EUA

3.10. Structure and Cell Viability Characterization by Fluorescence Microscopy

Fluorescence microscopy is a type of optical microscopy that may be used to check 3D spheroid structure and perform live/dead assays to check spheroid viability and layers distribution (Costa et al., 2016).

In the preparation of samples for fluorescence microscopy for structure analysis with staining of the membrane and nucleus, PC3 spheroids were fixed with a 4% PFA solution for 1 hour. The spheroids were then submerged in 37ºC CellMask Deep Red Membrane stain (Thermo Fisher Scientific, USA) for 15 minutes and after washed 3 times with PBS.

For the Annexin V/Propidium Iodide double staining they were submerged in a solution with 2.5 µL of Annexin V and 1 µL of propidium iodide (KIT Immunotech, Beckman Coulter, Czech Republic) and fixed after with a 4% PFA solution.

They were then carefully transferred from the multi-wells to slides with the assistance of the MagPen, where they were mounted with ProLong® Gold antifade reagent with DAPI (P36931, Life TechnologiesTM) and left to dry away from the light. The slides were then sealed and then subsequently observed in a fluorescence microscope Leica DM 4000 B.

3.11. Cell Death Populations and Viability Studies by Flow Cytometry

Necrosis and apoptosis are two forms of cell death and can be differentiated based on the morphologic, biochemical molecular characteristics of each process. Necrosis is a

disorganized process, which usually occurs in pathological conditions and that is characterized by the loss of integrity of the plasma membrane. On the other side, apoptosis is a programmed event, with the function of maintaining the homeostasis of the organism and that is characterized by maintaining the integrity of the membrane.

The Annexin V (AnV) is an anticoagulant protein that binds with anionic phospholipids, such as the phosphatidylserine. During apoptosis, it occurs the translocation of phosphatidylserine to the external layer of the cell membrane, and so apoptotic cells may be identified through the staining with AnV. On the other side, propidium iodide (PI) is a dye with the capacity of binding to the cell's DNA. In spite of this, this dye cannot get through the lipid bilayer, being only capable of binding to the DNA when the membrane is destroyed, event that can be verified when cells are in late apoptosis or necrosis (Wlodkowic et al., 2009).

To compare conditions, 2D cultured cells with more than 90% confluency at 7 days and 3D spheroids with 7 days cultured as referred above were used. Monolayer cultured cells were detached with the help of Tryple and the 3D spheroids were also broken down to individual cells with the assistance of a few drops of Tryple.

To perform this technique, it was used 1 million cells obtained after centrifugation at 1300 xG for 5 minutes. The obtained pellet was resuspended, washed in PBS and centrifuged again. After that, the PBS was discarded, and the resulting pellet was resuspended in 100 µL of binding buffer and incubated with 2.5 µL of AnV-FITC and 5 µL of propidium iodide (KIT Immunotech, Beckman Coulter, Czech Republic).

Subsequently, cells were excited at a wavelength of 494 nm for AnV-FITC and 351 nm for PI, collecting 10,000 events. Data were obtained using Cell Quest Software (Becton Dickinson) and analysed using of Paint-a-Gate software (Becton Dickinson).

3.12. Statistical Analysis

Statistical analysis was performed using the IBM® SPSS® Statistics software, version 24.0 (IBM Corporation, Armonk, USA), using a significance level of 5%. First, normal distribution and variance of the quantitative variables was assessed using Shapiro-Wilk and Levene tests, respectively.

By default, non-parametric tests were used when $n<10$. Differences with the control conditions were estimated by one-sample T test or Wilcoxon test, for parametric or non-parametric analysis, respectively. For comparisons of two cell culture methods or conditions, Mann-Whitney test was used or T student test in case of parametric analysis. Differences between more than two therapeutic conditions were performed using the parametric one-factor analysis of variance (ANOVA) or the non-parametric Kruskal-Wallis, followed by post-hoc analysis using Tukey correction (homogeneous variances).

CHAPTER 4 - RESULTS

4.1. Spheroids Characterization

Before testing the treatment with ^{223}Ra on 3D spheroids, it various assays were done to characterize the 3D structures, which is one of the main objectives of the experimental work. The magnetic levitation method was used to accomplish the 3D structures and two cell lines of metastatic prostate cancer, LnCap and PC3.

4.1.1. Spheroid evolution over time

The arrangement and growth of PC3 spheroids from plating over 6 days was accompanied with an inverted microscope and can be observed in Figure 17.

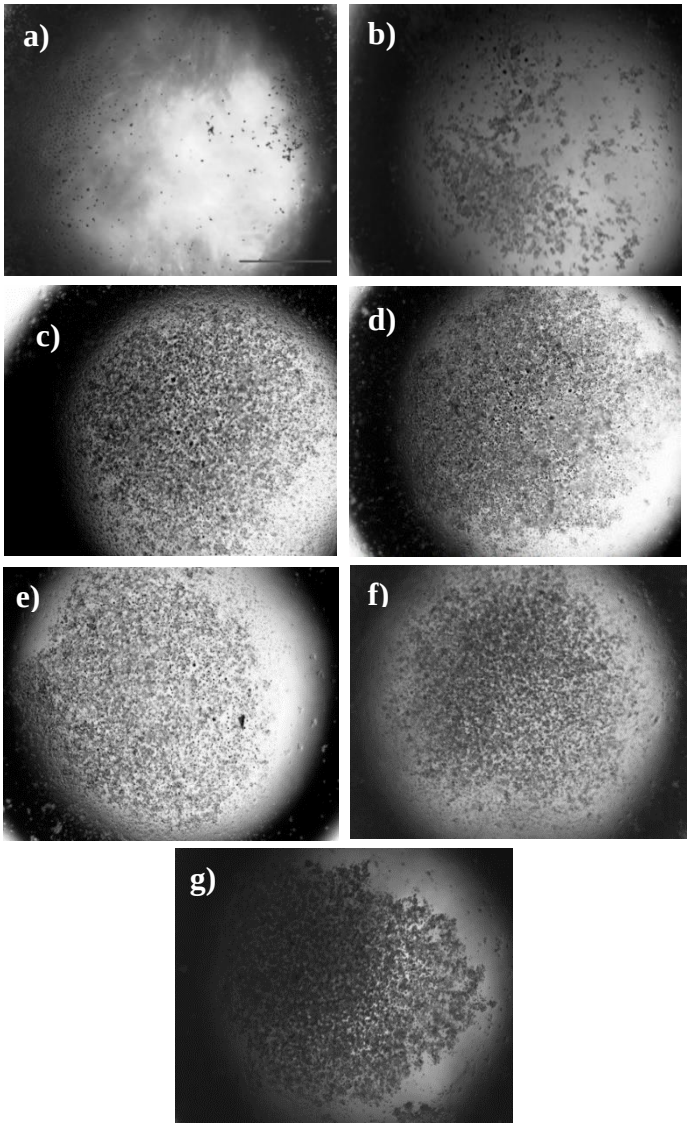

Figure 17: Representative images of PC3 3D spheroid arrangement and growing at 0 (a), 1 (b), 2 (c), 3 (d), 4 (e), 5 (f) and 6 (g) days after seeding. Images were all taken at 40x magnification and the scale at a) is equal to 1 mm.

In the 3D system, PC3 cells started to cluster 24 hours after seeding. Somewhere between 24 and 48 hours (between b) and c) in Figure 17) the majority of the cells were arranged to a big compact spheroid with a diameter larger than 2 mm and a mean area of 4.2 mm^2. The spheroid growth was accompanied with an inverted microscope and showed no relevant changes at the naked eye from 48 hours on, but with the analysis and estimation of the spheroids area represented in Figure 18 it was observed that there is a significant raise in the area between 3 and 4 days ($p<0.001$) and a significant decrease between 4 and 6 days ($p=0.026$).

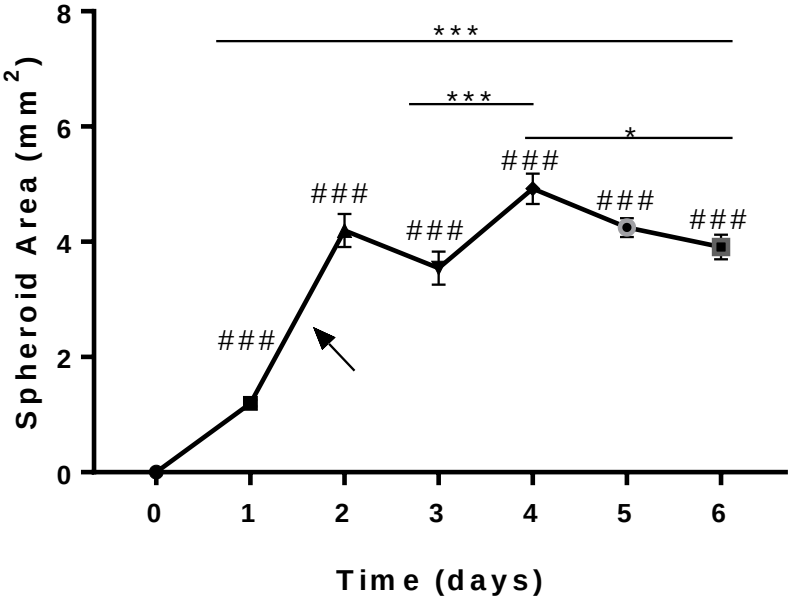

Figure 18: Growth curve of PC3 spheroids according to their areas. The arrow represents the time when only one compact spheroid is formed instead of various cell clustering. Results are expressed as mean and standard error of the mean (SEM) from n=6 of at least 3 independent experiments. Wilcoxon and Tukey test (### $p < 0.001$, in comparison to day 0 ; *** $p < 0.001$, * $p < 0.05$).

Besides PC3 cells, the 3D magnetic levitation technique was also performed with LnCap cells, which were also accompanied by inverted microscope imaging, represented in Figure 19. These showed to start 3D cultures with different morphology when compared to the PC3, forming smaller cell clusters and more dispersed levitated cultures, proving that not all cell types form the same type of spheroids. After this point, all experiments were performed with the PC3 cell line.

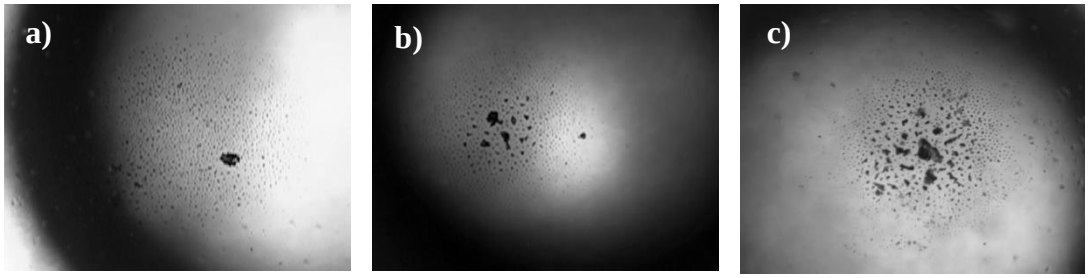

Figure 19: Representative images of LnCap 3D cultures clustering and growing at 1 (a), 2 (b) and 5 (c) days after seeding. Images were all taken at a 40x magnification.

4.1.2. Influence of the Magnetic Levitation Method on Cell Metabolism

To check if both the magnet and the NanoShuttle (NS) influence the cell's behaviour and metabolism in any way, it was made an MTT assay with monolayer cultured PC3 cells incubated either with magnets or NS. The results of these assays can be observed in Figure 20.

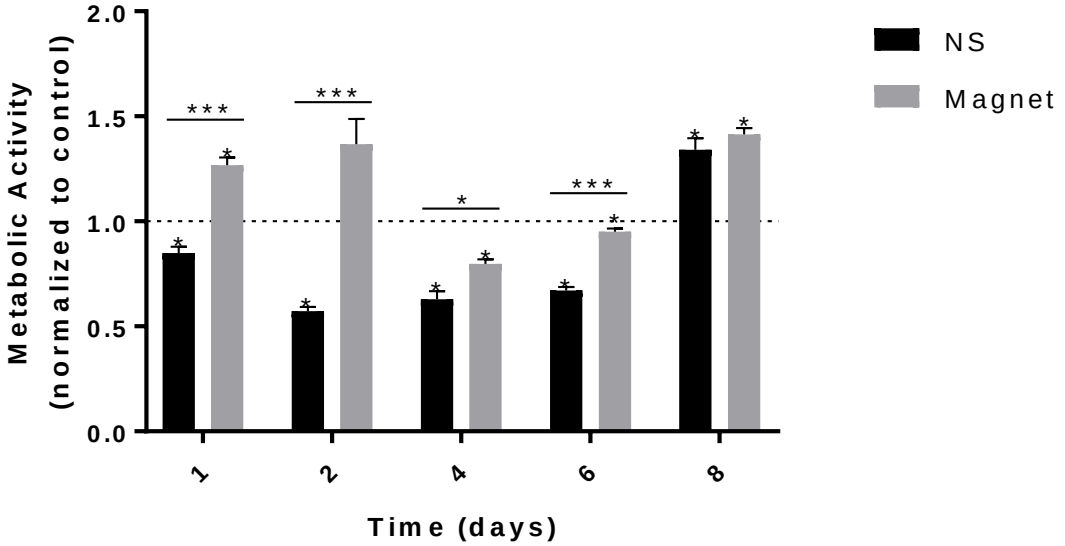

Figure 20: Evaluation of the cell's metabolic activity after the incubation with the magnets and NS. Data is normalized to the control and expressed as mean and SEM from n>6 of at least 3 independent experiments. Wilcoxon and Mann-Whitney U tests (*** $p < 0.001$, ** $p < 0.01$, * $p < 0.05$).

After 24h, the cells incubated with NS showed a significant decrease in the metabolic activity compared to the control ($p=0.011$), whereas the cells incubated with the magnet showed a significant increase in their metabolism ($p=0.012$). The same tendency was maintained at the 2-day mark, with cells showing an equal significant decrease with NS and increase with the magnets. On the other hand, at 4 and 6 days, cells presented a significant decrease in metabolic activity both when incubated with NS and the magnets, but always with the cells incubated with the magnets showing a significant increase when compared to the NS ($p=0.012$ and $p<0.001$). At 8 days, on the contrary, both the conditions had a significant increase in comparison to the control ($p=0.012$) but had no significant changes between them. So, it was concluded the NS had a significant lowering impact in the metabolic activity of the cells till the 6^{th} day, and the magnets at 4 and 6 days, but on the contrary, at 8 days both the conditions showed to have an increase in the metabolic activity compared to the control.

4.1.3. Spheroid Structure

The spheroid structure was qualitatively evaluated by two different methods, histochemical staining with toluidine blue and haematoxylin and eosin (H & E), which are represented in Figures 21 and 22 respectively, and by fluorescence microscopy, whose results can be observed in Figure 23.

4.1.3.1. Histochemical Staining

The toluidine blue is a basic thiazine metachromatic dye that has high affinity for nucleic acids, staining the DNA with blue. Looking at Figure 21, it can be observed the sphere-like form of the 3D spheroid of PC3 cells. It can be clearly identified regions stained with dark blue that are related with cells in high proliferation, and with light blue, which can denotate necrotic cells, having less nucleic acid coloration. The blackish coloration observed inside the spheroid is connected with the nanoparticle used in the magnetic levitation method.

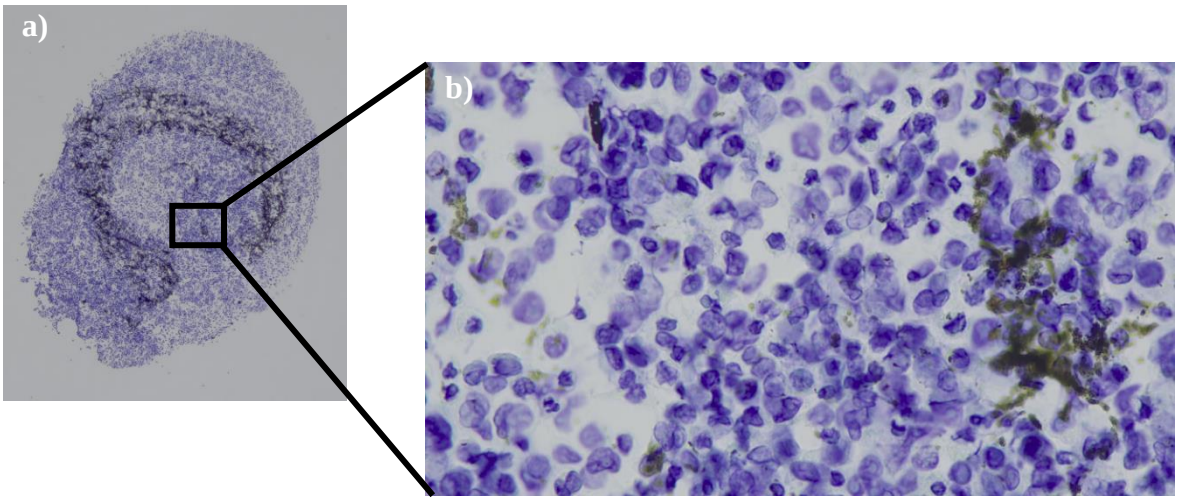

Figure 21: PC3 3D spheroid stained with toluidine blue with 40x (a) and 400x (b) magnifications.

The haematoxylin and eosin coloration is one of the most used colorations in histology. The haematoxylin has a deep purple staining and also has affinity with nucleic acids, whereas the eosin has a pink color and is highly affined with the cytoplasmic proteins. After performing a smear with the cells of a 3D spheroid (represented in Figure 22), it was able to perceive dark purple regions, constituted by cells with a high rate of proliferation, light pink regions, which are normally more a sign of late apoptotic or/and necrotic cells, and the nanoparticle traditional blackish regions.

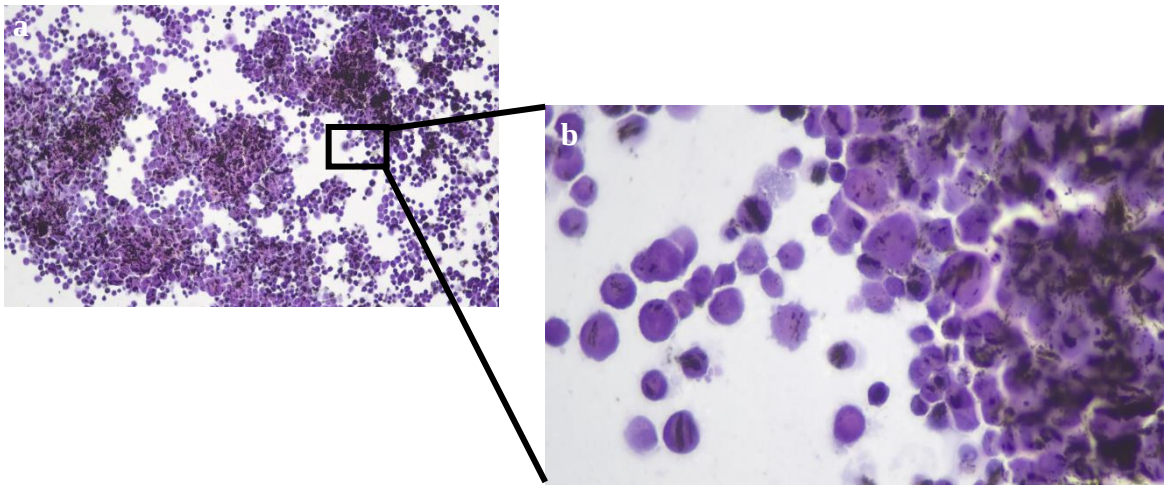

Figure 22: PC3 3D spheroid smear stained with haematoxylin and eosin with 40x (a) and 400x (b) magnifications.

4.1.3.2. Fluorescence Microscopy

Besides the histochemical staining, it was also performed fluorescence staining and microscopy to check the spheroid and cell structure, whose results also showed a spherical form in the 3D spheroids and are exposed in Figure 23.

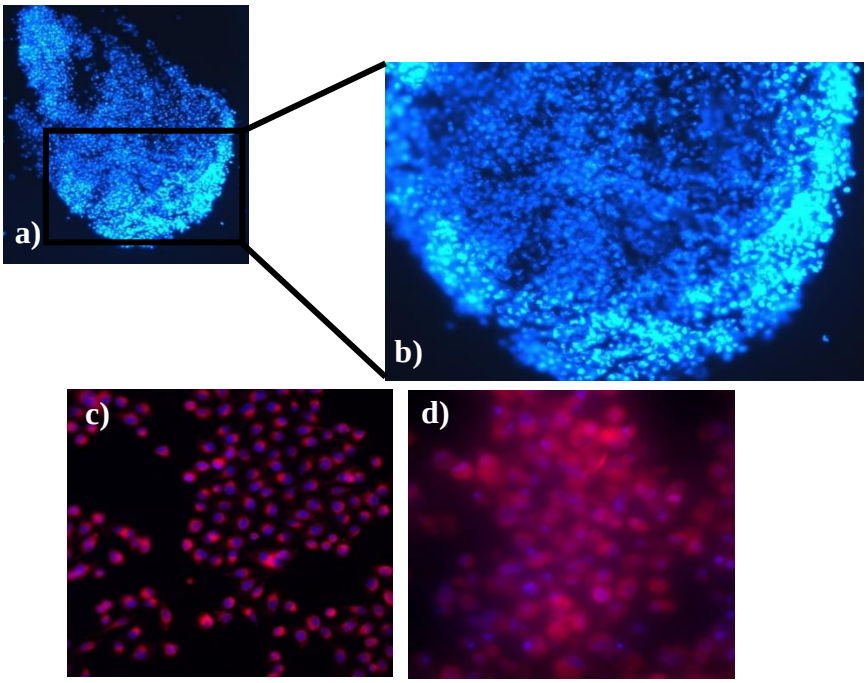

Figure 23: Representative images of spheroid structure in PC3 3D structures (a, b, d) when compared to cells cultured in monolayer (c). a) and b) were stained with DAPI, and c) and d) were stained with DAPI and CellMask for membrane. Images were taken in a fluorescence microscope with 40x (a), 100x (b) and 200x (c, d) magnifications.

4.1.4. Protein Markers Presence

To evaluate and characterize qualitatively protein expression in the 3D spheroids [Figure 24 b), d), f), h) and j)], it was performed immunocytochemistry as described above, using monolayer cultured cells as a term of comparison [Figure 24 a), c), e), g) and i)]. It was assessed the expression of 5 proteins (KI-67, P16, caspase 3, vimentin and P53) and the results are presented in Figure 24. The proteins chosen are related with cell proliferation (KI-67), cell death and DNA damage (caspase 3 and P53), senescence (P16) and cell structure (vimentin).

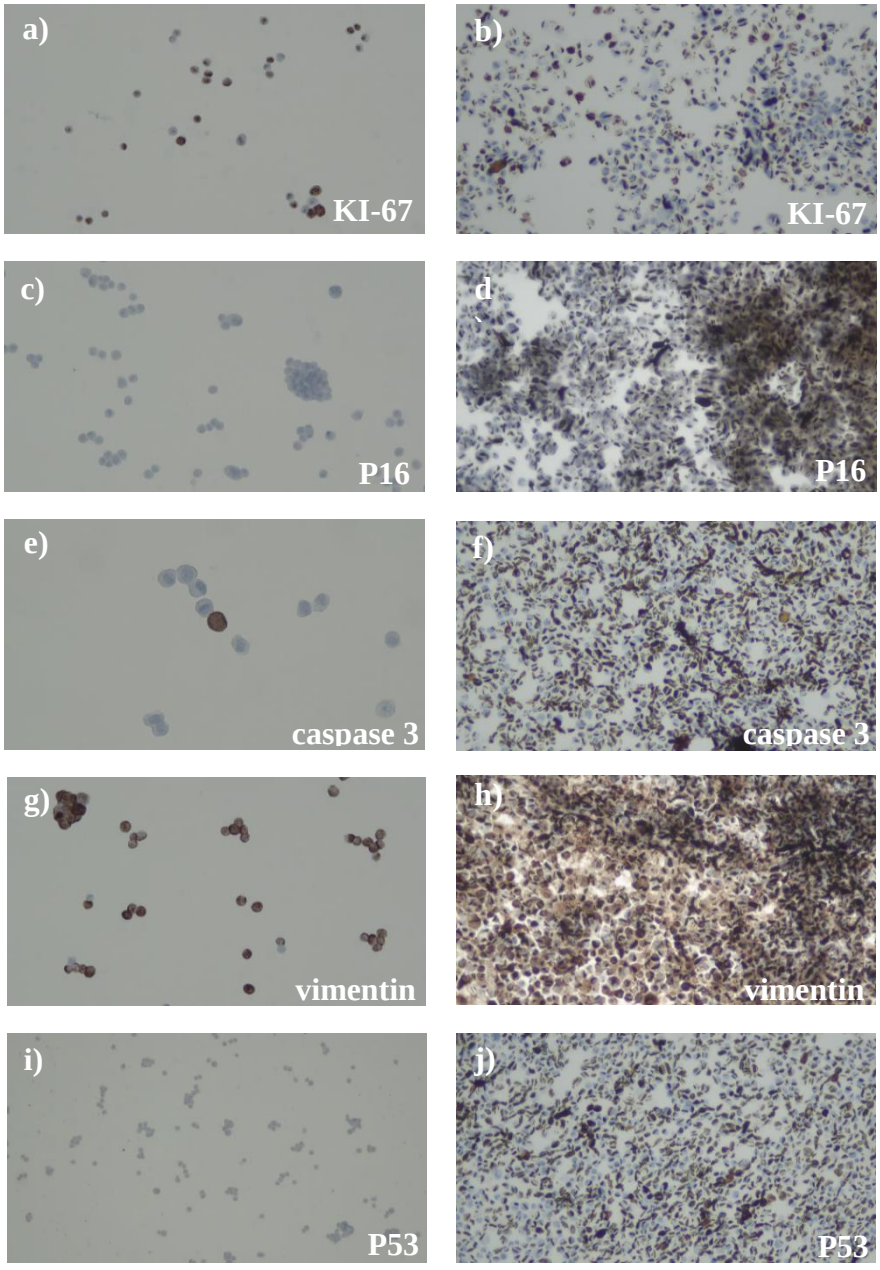

Figure 24: Immunohistochemical staining on 2D monolayer (a, c, e, g, i) and 3D spheroid (b, d, f, h, j) cell culture modes. The illustrated samples were stained for KI-67 (a, b), P16 (c, d), caspase 3 (e, f), vimentin (g, h) and P53 (i, j). Images were taken using an optic microscope with 100x and 200x magnification.

Comparing qualitatively monolayer smears with the 3D spheroids, it can be seen a decrease in the number of cells expressing the KI-67, whereas the P16 protein is not present in the 2D cultured cells but it is present in some cells cultured in three dimensions, mostly in the spheroid's internal layers, although most of the antibody staining is not specific. In the case of caspase 3, it was detected in a few cells in monolayer but has a higher cytochemical signal in the spheroid's cells. Regarding the vimentin, it is heavily expressed both in monolayer and in the spheroids, but the staining appears to be even stronger in the 3D cultures. Finally, no expression of P53 was detected in the 2D cells, but in the spheroid some cells expressed this protein. Information relative to the semi-quantitative analysis for both conditions, which was based on comparing the number of cells that marked for each protein, can be observed in Table 3.

Table 3: Resume of the immunocytochemical staining pattern: positive staining (++), mild staining (+) and minor to negative staining (-).

Immunocytochemical Staining	Monolayer	Spheroid
KI-67	++	+
P16	-	+
Caspase 3	-	+
Vimentin	++	++
P53	-	++

4.1.5. Cell Viability and Death Populations

Cell viability and cell death pathways, as described previously in the methods, were evaluated with double staining with Annexin V and Propidium Iodide (AnV/PI) qualitatively by fluorescence microscopy and quantitatively by flow cytometry. This staining allows to differentiate the existing cellular populations: viable cells, initial apoptosis, late apoptosis/necrosis and necrosis. These two assays allowed to characterize and evaluate the type of cell death induced in the cells when these are cultured in 3D spheroids.

The qualitative evaluation of cell viability and cell death pathways was performed by fluorescence microscopy, staining the cell's nucleus with DAPI and a double staining with AnV/PI. These results can be observed in Figures 25 and 26.

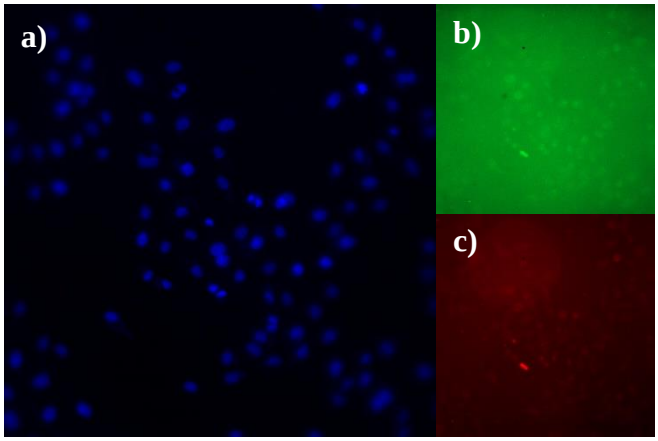

Figure 25: Representative images of DAPI (a), AnV (b) and PI (c) stained 2D monolayer cultured PC3 cells. Images were taken in a fluorescence microscope with 100x magnification.

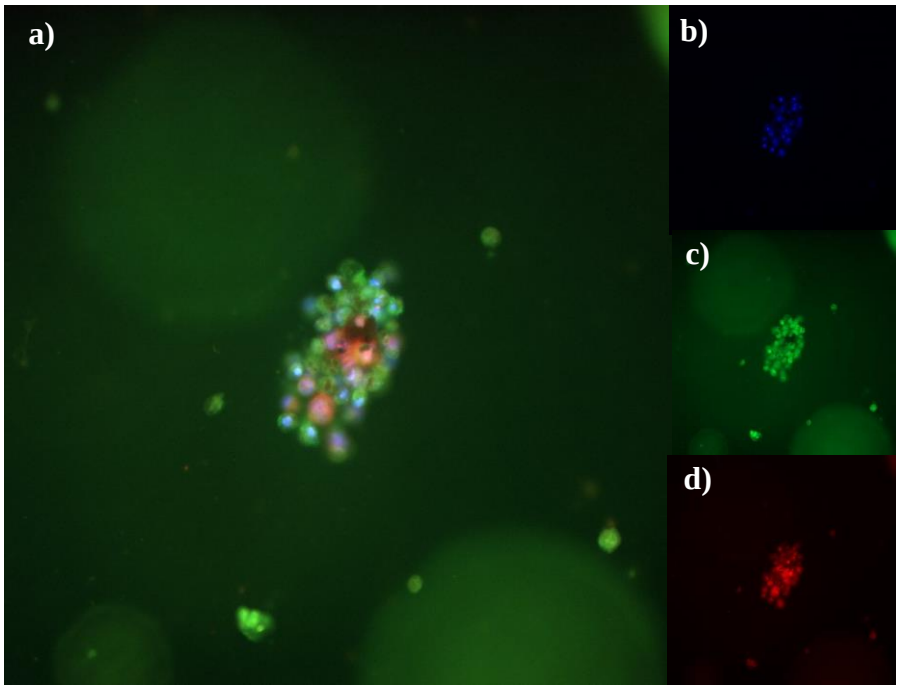

Figure 26: Representative images of merged (a), DAPI (b), AnV (c) and PI (d) stained 3D spheroid PC3 cells. Images were taken in a fluorescence microscope with 100x magnification.

In the fluorescence microscopy studies, the cells cultured in 2D (Figure 25) showed normal nucleus, with almost no staining either with the Annexin V and the PI, whereas the

spheroids (Figure 26) showed mild staining with the Annexin V and strong staining with the PI, showing a strong presence of late apoptotic or necrotic cells in the spheroid.

After qualitatively evaluating and comparing 2D and 3D PC3 structures by means of fluorescence microscopy, it was needed to have quantitative data so that conditions could be better compared and characterized. The evaluation of cell viability and death populations by flow cytometry for the characterization of the 3D model allowed the obtaining of the results presented in Figure 27.

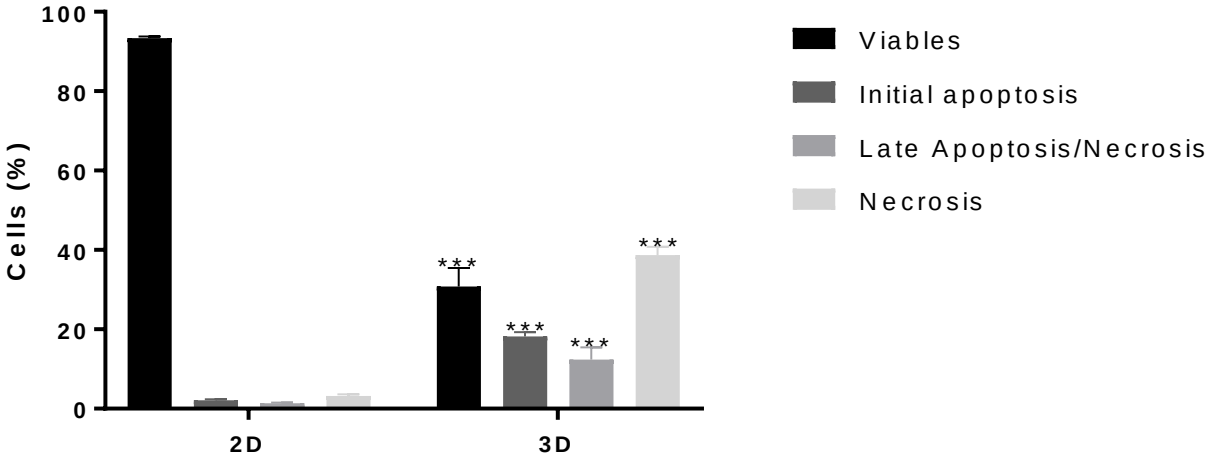

Figure 27: Viability and cell death pathways evaluation by flow cytometry. The results were obtained with PC3 7-day monolayer cultured cells (2D) and spheroids (3D). The results are expressed as percentage of viable cells, in apoptosis, late apoptosis/necrosis and necrosis, and represent mean and SEM from n>6 from at least 3 independent experiments. Mann-Whitney Test (*** $p < 0.001$).

As observed, the viable cells population showed a statistically significant decrease ($p=0.0003$) from 93±0.44% in the 2D model to only 32±4.09% in the 3D model of spheroids with 7 days of culture. Concerning the cell death pathways, the spheroids show a significant increase in the population of cells in initial apoptosis (2±0.26%) in relation to 2D (18±1.09%) ($p=0.0003$). This increase of dead cells was also observed in the population of cells in late apoptosis or necrosis ($p=0.0002$), from 2±0.17% to 12±3.13%, and also in the necrotic population, where the highest raise was observed, with spheroids presenting 38±2.09% of necrotic cells when comparing to the 3±0.40% in the monolayer cultured cells ($p=0.0002$). These data supports the one taken from the fluorescence microscopy studies, where an increase in apoptosis and especially in necrosis was also observed in the 3D spheroids.

4.2. Treatment of Spheroids with Radium-223

In order to evaluate the effects of ^{223}Ra in PC3 3D spheroids, it was performed the alamar blue assay, which evaluates the cell proliferation indirectly through metabolic reactions, the SRB assay, which evaluates the total protein content, and the May-Grünwald-Giemsa staining, which was used to describe the morphologic changes in the cells before and after the irradiation.

4.2.1. Cell Proliferation

Cell proliferation 48 hours after irradiation with ^{223}Ra was evaluated with the alamar blue assay in doses of 1, 4, 10, 15 and 20 mGy. These results can be observed in Figure 28.

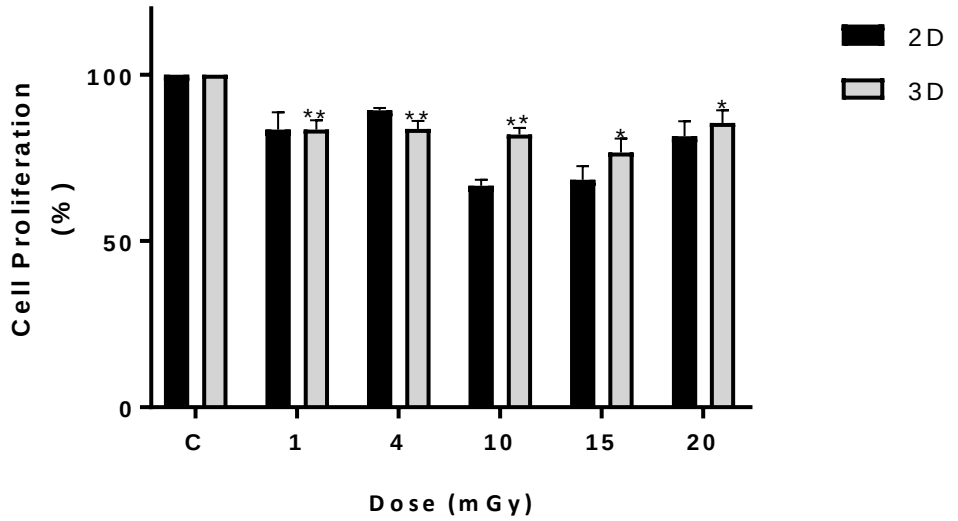

Figure 28: Evaluation of the cell proliferation by the alamar blue assay 48 hours after the irradiation with ^{223}Ra with doses of 1, 4, 10, 15 and 20 mGy both in monolayer cells (2D) and spheroids (3D). Results are normalized to control and expressed as mean and SEM from n>9 from at least 3 independent experiments (2D is only n=3 from 1 independent experiment). Wilcoxon test (** $p < 0.01$, * $p < 0.05$)

Concerning the cell proliferation 48 hours after irradiation with ^{223}Ra, it showed a tendency to decrease with increasing the doses of ^{223}Ra in 2D cultured cells. A slight tendency to cell proliferation increase is observed for 20 mGy irradiation, when compared to lower doses, however all without statistical significance. Regarding the 3D spheroids, these showed a statistically significant decrease in all 5 doses when compared to the control, presenting decreases to 83,6±2.71% (p=0.002), 83,8±2.33% (p=0.003), 82,1±1.94%

(p=0.005), 76,7±%4.22 (p=0.012), and 85,6%±3.78 (p=0.018). As observed for 2D culture, for the 20 mGy dose an unexpected increase in cell proliferation was also observed when compared to lower doses, but without statistical significance. Comparing the two different culture methods, there were no significant changes, however in general greater differences on cell proliferation after irradiation are seen in the 2D culture, when compared to the 3D spheroid, in all doses but 4 mGy.

4.2.2. Protein Content

The SRB assay is a technique used to evaluate the total protein content of the cells, which is proportional to the cell proliferation, and so we are able to evaluate the cytotoxicity degree of a certain therapeutic agent. The objective was to use this assay to evaluate the effects of 223Ra on PC3 3D spheroids, 48 hours after irradiation in a dose of 10 mGy, and then compare the results with previous ones in monolayered cultured cells. These results can be observed in Figure 29.

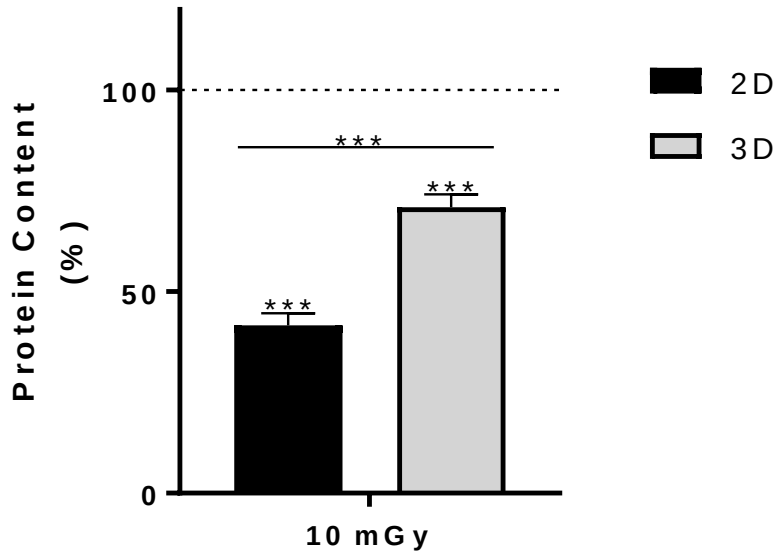

Figure 29: Evaluation of the protein content by the SRB assay, 48 hours after the irradiation with ^{223}Ra with a dose of 10 mGy in both monolayer cells (2D) and spheroids (3D). Results are normalized to control and expressed as mean and SEM from n>9 from at least 3 independent experiments. T student test and one sample T test (*** $p < 0.001$)

Regarding the protein content, it was observed a significant decrease (p=0.0004) in monolayer 2D cells 48 hours after irradiation with a dose of 10 mGy, since it dropped

58.3±2.99% when compared to the control. In the 3D spheroids, there was also a significant decrease (p=0.0003) in the protein content compared to the control but only 29±3.17%. Comparing the irradiation with the same dose but with different culture methods, there is a significant decrease in protein content in the 2D cells when compared to the 3D cells of the spheroid (p<0.0001).

4.2.3. Cell Morphology

Besides the alamar blue and SRB assays for proliferation and total protein content studies, respectively, it was performed the morphological characterization of the spheroid cells irradiated with ^{223}Ra by May-Grünwald-Giemsa staining. In Figure 30, it can be observed the representative images of the obtained results. The control cells present a round morphology but it also can be observed some necrotic cells, which are characteristic of the 3D model. In 1, 4 and 10 mGy doses, it can be noticed an increase in necrotic cells (green arrows) and some blebbing (red arrows) which can be an early sign of apoptosis, but it is difficult to assess if the damage was done by the ^{223}Ra or by the 3D model, due to the cell death already presented in the control.

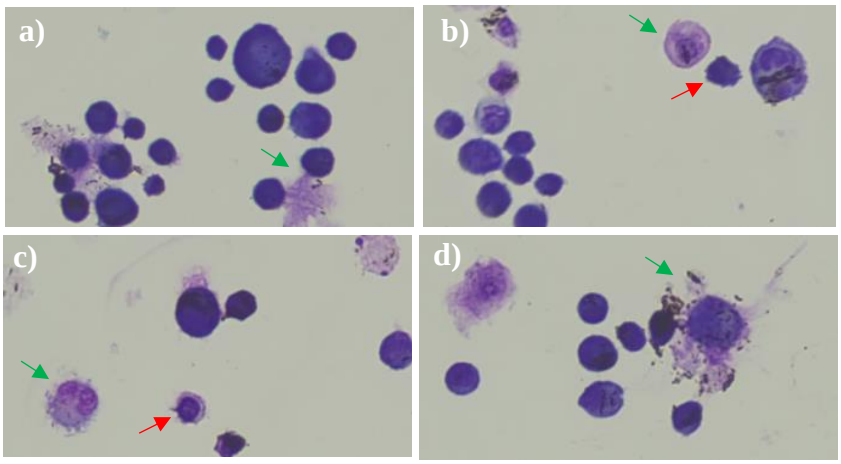

Figure 30: Representative images (400x) of morphologic features in PC3 spheroid cells post irradiation with ^{223}Ra, after cells staining by May-Grünwald-Giemsa staining. Control (a), 1 mGy (b), 4 mGy (c) and 10 mGy (d). Red arrows correspond to blebbing and green arrows to necrotic cells.

CHAPTER 5 - DISCUSSION

In spite of all the advancements in diagnosis and therapy in these past years, prostate cancer is still the second most frequently diagnosed and the fifth most mortal cancer in men (Bray et al., 2018). Due to these facts, this neoplasia is still a major concern in the world health panorama (Borley and Feneley, 2009; Bray et al., 2018).

Since the discovery of the hormone dependency present in the disease, advanced prostate cancer has been treated with androgen deprivation therapy, treatment that causes resistance to the chemical castration after a certain period, usually of 3 years or less (Harris et al., 2009). This phase of the disease is designated as "castration resistant prostate cancer" and still remains uncurable (Fujita and Nonomura, 2018).

Bone metastasis are responsible for the presence of skeletal-related events such as intense pain and mobility loss, which lead to the patient's loss of life quality, and they still lack appropriate therapeutic solutions capable of retarding the appearance of these symptoms (Lassi and Dawson, 2009).

^{223}Ra was the first alpha particle emitter radioisotope accepted for therapeutic, and it was approved for the treatment of patients with castration-resistant metastatic prostate cancer with the presence of known bone metastases and no sign of visceral metastasis (Jacene et al., 2018; Smith et al., 2019). The high LET associated to the alpha particles induces an elevated frequency of DNA double strand breaks, which results in an anti-tumor effect on bone metastasis (Liberal et al., 2017). These alpha particles have the advantage of having a short range, which limits the damage on adjacent normal tissues (Lewington, 2005).

In monolayer culture, the PC3 cells show to be radiosensitive to ^{223}Ra at very low doses, around 4 mGy, according to a clonogenic assay previously performed, and due to that, the necessary dose to induce cell death on 50% of the cellular population presents a very low value (Marques, 2016). The clonogenic assay also showed that Radium-223 showed a linear model of cellular aggression (Marques, 2016). The linear model is based on the theory that in the cell there are especially important targets such as the DNA, that, when damaged, are enough to induce cell death and trigger an independent response (Lewington, 2005). These results go accordingly to the described in the literature, since alpha particles present high values of LET provoking higher incidence of cell death, with few opportunities for DNA damage repair (Liberal et al., 2017; Lassmann and Eberlein, 2018).

Subsequently, with our study we wanted to contribute, in a first phase, to optimize a 3D model of prostate cancer, and then to treat 3D spheroids with Radium-223. We also wanted to help to have a better knowledge about the molecular mechanisms and effects of this radiopharmaceutical in 3D structures of prostate carcinoma cells, in a way that it can enable a better application and potential of this treatment in the clinical approach.

Related to the 3D optimization technique using the magnetic levitation method, one of its disadvantages is that for culture cells a coloured magnetic particle is used. This magnetic nanoparticle, which is necessary for keeping the cells in levitation with the action of the magnetic field, can in histochemical and immunohistochemical assays hamper the analysis of the microscopy images, because it can be confounded with the DAB (3,3′-Diaminobenzidine), due to the fact that they both have a brown coloration (Haisler et al., 2013). To prevent this limitation, in the future it is recommended to use a colorimetric marker with another staining color, such as the 3-amino-9-ethylcarbazole, which turns the staining red when reacting with alkaline phosphatase, or to use fluorescence microscopy, because the nanoparticle does not tamper with this method (Haisler et al., 2013; Jaganathan et al., 2014).

In 2014, Tseng and colleagues used the magnetic levitation method to achieve a co-culture model of the aortic valve. In this study, the authors reported that both cells lines used by them did not present significant metabolic differences when cultured in monolayer and incubated with NanoShuttle and the magnet (Tseng et al., 2014). Our results showed significant differences when the metabolism of control cells was compared with the cells incubated with the NanoShuttle™ and the magnet alone, especially the NanoShuttle™. However, on day 8, both conditions showed higher metabolic activity when compared to the control. So, although the cells appear to show some response to the nanoparticle in the first days, over time they seem to recover and at 8 days still present higher metabolic activity when compared to the control. The use of the magnet in 2D-cultured cells showed almost no effect on the cells metabolism, which goes accordingly to the literature, because in the magnetic levitation method it is used a magnet with a magnetic field of 30-500 Gauss (G), which has no effect on cell proliferation, metabolism and does not trigger any inflammatory response (Haisler et al., 2013).

Comparing the cell structures formed by each cell line, PC3 and LnCap assembled very different types of 3D structures, in terms of morphology. PC3 cell line, which is from a bone metastasis of prostate cancer, formed a single spheroid after 24 to 48 hours of culture with the magnetic levitation method. In contrast, LnCap, a cell line derived from a lymph node metastasis of prostate cancer, was shown to form smaller and more dispersed 3D structures, more like small cell clusters, structures that are also common when these cells are cultured in monolayer (Haisler et al., 2013; Takir, Debelec-Butuner and Korkmaz, 2018). This difference may be due to their different origin, from different metastatic microenvironments. PC3 cells are from bone tissue, a dynamic but more rigid structure, which could be reflected in a more compact spheroid. LnCap cells are derived from the lymph node, with a clear tendency to form smaller dispersed cells clusters due to the fact that their tumor microenvironment is more liquid (Seim et al., 2017). This difference between the two cell lines in terms of 3D structures made us opt to move on with the PC3 cell line, due to their more compact spheroid conformation.

Concerning the area of the PC3 spheroids, our results showed that after the formation of the compact structure between 24 and 48 hours after seeding, the area suffered an increase until the 4 days of culture, which could be a sign of some cell proliferation and more levitated cells joining the spheroid. However, the area of the spheroids decreased for longer periods, namely between 4 and 6 days, which might be due to cell death processes (afterwards verified in the flow cytometry studies), as well as, spheroid cellular contraction.

According to Jaganathan and colleagues, a breast cancer 3D structure took about 24 hours to form with the magnetic levitation method, faster when compared with other methods to form 3D structures, such as Matrigel. The formation of the tumor structure using another type of methods usually only allow to form structures of the same magnitude 7 days after seeding (Haisler et al., 2013).

The formation of 3D cancer structures in the range of mm^2 is very important for the study of hypoxic and necrotic areas in tumors. The magnetic levitation method is performed on 6 and 24-well plates and allows achieving structures of this scale, allowing the study of these tumor characteristics (Becker and Souza, 2013; Jaganathan et al., 2014).

The immunocytochemical studies showed a decrease in the KI-67 staining, a proliferation marker. In fact, this is expected, especially in spheroids of this magnitude. In

large spheroids only the cells in the periphery are supposed to proliferate, while the others, located in the inner layers of the spheroid, are supposed to be either senescent or in necrosis, which justifies the KI-67 non-staining (Monazzam *et al.*, 2007; Li *et al.*, 2015).

The cell cycle is a crucial parameter to have in account in terms of cell proliferation. The P16 is a protein that plays a very important role in the cell cycle, more specifically by slowing the cycle progression from G1 to S phases (Liggett and Sidransky, 1998). The increase of this protein expression in the spheroids might be related to the existence of a layer of senescent cells in the PC3 spheroids produced in the study (Althubiti et al., 2014).

On the other side, P53 is a tumor suppressor protein and plays a major role in the cellular response to DNA damage, and is one of the most studied proteins in the context of cancer, also being known as the "guardian of the genome" (Toufektchan and Toledo, 2018). The increase in the expression of P53 in the 3D structures might have to do with the prevention of proliferation of cells that have damaged DNA, caused by the model itself. As observed in the flow cytometry studies, apoptotic and necrotic zones were clearly observed (He et al., 2016).

The apoptosis, also designated programmed cell death, is a mechanism where the cell is self-destructed when it is triggered by certain stimulate (Elmore, 2007). The caspase-3 is a key regulator protein in the process of apoptosis. Thus, the raise in the expression of this protein in the 3D spheroids when compared with the monolayer is most likely due to the increase of apoptotic cells in the 3D model (Mittler et al., 2017; Pu et al., 2017).

Finally, the last studied protein was vimentin, which is a major constituent of intermediate filaments and has a highly important role in cell structure integrity and resistance against stress (Satelli and Li, 2011). This protein showed very high expression in both 2D and 3D cultured PC3 cells, which goes accordingly to the literature, whose information states that vimentin is associated with cells of bone metastasis in prostate cancer. In contrast, the downregulation of this protein in PC3 cells lead to a decrease in their invasive capacity (Singh et al., 2003).

Besides serving protein expression characterization of the spheroid, these assays should also be performed with ^{223}Ra treated spheroids, to check the changes in the expression of key proteins.

According to Gebhard and colleagues, and Riffle and colleagues, spheroids start to show necrotic phenomena in their core region with diameters above 300 µm (Gebhard et al., 2016; Riffle et al., 2017). The spheroids obtained by us with the magnetic levitation method were much larger, having diameters bigger than 2000 µm. Thus, a necrotic core should be expected in a spheroid of this magnitude, even changing its culture medium every day, due to the fact that its form and size don't let the oxygen and nutrients to reach the spheroid's inner layers, causing the cells to enter in a state of low oxygen partial pressure, a condition that can lead to senescence or necrosis (Costa et al., 2016; Sant and Johnston, 2017). Although this is effectively an approximation of what happens in an *in vivo* tumour, we can't induce angiogenesis in a spheroid of this type and with a low cell viability in the spheroids (even the control 3D spheroids, as enlightened by the flow cytometry studies performed for cell viability and death pathways) it becomes difficult to measure and compare the effectiveness of a certain therapy, in this case the ^{223}Ra. An active solution would be to grow smaller spheroids either in 48 or 96-well plates and test the therapy before they start to display necrotic cores, below 300 µm (Haisler et al., 2013; Gebhard et al., 2016).

From a certain diameter, a tumor can only grow if it has an effective vascularization network for the delivery of oxygen and nutrients to its cancer cells (Roato, 2013). In case this doesn't happen, the tumor cells go into hypoxia, upregulating HIF1-α and having clinically relevant consequences such as chemical and radioresistance and poorer prognosis for the patients (Riffle et al., 2017). Hypoxia can induce genomic and proteomic changes in cancer cells (Muz et al., 2015). These changes can stimulate the tumor growth, invasion and metastisation facilitating the survival of the malignant cells in a hostile and nutrient-deprived environment (Tameemi *et al.*, 2019).

These data are still preliminary and needs further optimizing and research namely using other ^{223}Ra doses and incubation times with perhaps smaller spheroids to raise their cell viability and diminish or eliminate their necrotic cores. However, it is important to highlight the fact that the SRB results obtained with 10 mGy at 48 hours after irradiation displayed a significantly decreased sensitivity of the PC3 spheroids to the radiopharmaceutical, which can mean that 3D cultured cells create more realistic scenario when compared to *in vivo* and have decreased toxicity to the treatment (Babel et al., 2017). This makes sense considering that alpha particles, such as the case of ^{223}Ra, although possessing a high LET, present a very limited penetration range in the tissue, more or less

100 µm, and the spheroid's diameter was in the range of 2 mm, which is several times the predicted ^{223}Ra penetration range, and so the treatment probably might not be reaching all the cells in the spheroid (Marques et al., 2018).

Cells cultured in 3D demonstrate a different behaviour pattern when compared with those cultured in monolayer, namely in what concerns to, matrix adhesion, cell polarity, protein expression, proliferation and migration (Nyga, Cheema and Loizidou, 2011; Carvajal et al, 2012). Concerning the exposure of cells to irradiation with ^{223}Ra, the monolayer cultured cells are all equally exposed to the treatment, whereas in the 3D model, cells are differently exposed accordingly to their distances to the center of the spheroid, diminishing the treatment's effectiveness (Costa et al., 2016). According to previous studies in which authors compared treatment effects in 2D and 3D cell structures, results show lesser drug effects in 3D tumor spheroids when compared with their effects on cells cultured in monolayer (He et al., 2016; Kapałczyńska et al., 2018).

Thus, the differences between 2D and 3D cultures must always be taken into consideration when talking about cytotoxicity, either for chemo or radiotherapy. Regarding the alamar blue results, like the SRB ones, these also show a tendency to lower efficacy of the ^{223}Ra therapy in 3D cultures when they are compared with the 2D 48 hours after irradiation. Although in this case, 2D cells' sensitivity to Ra-223 is less accentuated and there are not statistically significant differences, this fact is mostly due to the fact that the 2D experiment was only performed once, and it needs a more robust number of independent experiments to give more satisfying results. Regarding the 3D-cultured cells, the values are statistically significant, and show a decrease in cell proliferation in all doses when compared to the control. Besides, results also show a tendency to higher proliferation values for higher doses (15 and 20 mGy), which could be a sign of an acquired radioresistance by the cells. A strategy to overcome this lower efficacy in the treatment of the 3D spheroids would be to give a number of daily doses of ^{223}Ra to the spheroids over an establish period of time, like it is performed in the clinic, and check the treatment's effectiveness and spheroid's viability and proliferation (Parker et al., 2013; Deshayes et al., 2017).

Finally, May-Grünwald-Giemsa staining allowed to check cell morphology aspects both in control and irradiated 3D cells. The results showed an apparent increase in the number of necrotic and apoptotic cells in the highest irradiation dose (10 mGy) and didn't

show noticeable differences in the lower doses. This is in agreement with the previous results, since the control cells already showed some cell death that was inherent to the 3D model, fact that made it hard to say with certainty which cells suffered damage due to the model and which damage was provoked by the effects of the irradiation. This raise in the number of necrotic cells after irradiation had already been verified in studies made with the same cell line after irradiation with ^{223}Ra in monolayer cultured cells (Marques, 2016).

CHAPTER 6 – CONCLUSIONS AND FUTURE PERSPECTIVES

The execution of this experimental work had as principal objectives the obtainment, optimization and characterization of a 3D cell culture model with two prostate carcinoma cell lines from different metastasis microenvironments, PC3 (bone) and LnCap (lymph node), and then the evaluation of the model's response to ^{223}Ra in the PC3 spheroids, and its effects in cell survival, morphology and total protein content by various molecular and cellular biology techniques.

The two cells lines showed to form different types of 3D structures, with PC3 showing to form a compact spheroid and LnCap establishing various cell clusters, fact that could be normal since they are from different metastatic environments and present different cell morphology.

Regarding the magnetic levitation method's influences on the PC3 cell metabolism, the results showed some significant changes on the metabolism in the first days, especially cause by the nanoparticle, but after 8 days the cell's metabolism even showed a significant increase either with the nanoparticle and the magnet, which could mean that both conditions do not have major biological influence on the model and its viability.

In the process of the spheroid's characterization, the protein expression analysis showed key protein expression changes between the 2D and 3D cultured cells, providing important information on the differences and the value amongst these two types of cultures, although to further analyse key proteins it is important to perform a Western blot assay which can give quantitative information on protein expression. Besides, there was a clear increase in the percentage of apoptotic and necrotic cells in the 3D spheroids when compared with the cells cultured in monolayer, which are most likely due to the model itself, with the creation of senescent and necrotic layers inside the spheroid due to its size and conformation.

After the characterization of the spheroids, it was evaluated the effects of the ^{223}Ra in the spheroids. Post irradiation, all doses tested showed significant decreases on total protein content and cell proliferation in the 3D cultures. Comparing these results to those of the irradiation with ^{223}Ra of monolayer cultured cells, it was noticed a significant change in the treatment's efficacy, which might be due to an approximation to the *in vivo* scenario of

the 3D model, decreasing the cytotoxicity of the radiopharmaceutical. In the future, these data should be replicated for more doses and incubation times after irradiation.

Subsequently, as future perspectives of the work, it is needed to further optimize the 3D spheroids, with lesser size to decrease necrotic zones and better evaluate the therapy. It is also considered that the creation of a cutting protocol of the spheroids would be a high-value resource, to better evaluate protein expression and the different layers present in the 3D structures with fluorescence or confocal microscopy, which are the best suited methods due to the color of the nanoparticle used in the magnetic levitation method. After these optimizations, it is needed to repeat the SRB assay for more doses and incubation times after irradiation to check if there are major changes, and in the future evaluate the direct damage of ^{223}Ra on DNA damage, and the indirect effects, with the production of reactive species of oxygen. With these studies in 3D structures, it is pretended to approach the effects of ^{223}Ra to their counterparts *in vivo*, get a better knowledge of the molecular processes involved and potentiate the use of this radiopharmaceutical in the clinical panorama.

Also, after the optimizing the model for separate cell lines (PC3 and LnCap), it is intended to co-culture each line with a cell line from its metastatic microenvironment, in this case, PC3 with an osteoblast cell line (hBOF-1.19), and LnCap with immortalized lymphocytes, to check the effects of the radiopharmaceutical in a more realistic microenvironment with tumor stroma.

CHAPTER 7 - REFERENCES

Aaron L, Franco O, Hayward SW (2016) Review of Prostate Anatomy and Embryology and the Etiology of BPH. Urol Clin North Am 43:279–288

Adhyam M, Gupta AK (2012) A Review on the Clinical Utility of PSA in Cancer Prostate. Indian J Surg Oncol 3:120–129.

Al Tameemi W, Dale TP, Al-Jumaily RMK, Forsyth NR (2019) Hypoxia-Modified Cancer Cell Metabolism. Front cell Dev Biol 7:1–15

Althubiti M, Lezina L, Carrera S, Jukes-Jones R, Giblett SM, Antonov A, Barlev N, Saldanha GS, Pritchard CA, Cain K, Macip S (2014) Characterization of novel markers of senescence and their prognostic potential in cancer. Cell Death Dis 5:e1528–e1528

American Cancer Society (2016) Cancer Facts & Figures 2016. Am Cancer Soc Inc.

Babel L, Grunewald M, Lehn R, Langhans M, Meckel T (2017) Direct evidence for cell adhesion-mediated radioresistance (CAM-RR) on the level of individual integrin β1 clusters. Sci Rep 7:3393

Bancroft JD, Gamble M (2008) Theory and Practice of Histological Techniques. Elsevier Health Sciences.

Becker JL, Souza GR (2013) Using space-based investigations to inform cancer research on Earth. Nat Rev Cancer 13:315–327.

Boorjian SA, Karnes RJ, Rangel LJ, Bergstralh EJ, Blute ML (2008) Mayo Clinic Validation of the D'Amico Risk Group Classification for Predicting Survival Following Radical Prostatectomy. J Urol 179:1354–1360.

Borley N, Feneley MR (2009) Prostate cancer: Diagnosis and staging. Asian J Androl 11:74–80.

Bray F, Ferlay J, Soerjomataram I, Siegel RL, Torre LA, Jemal A (2018) Global cancer statistics 2018: GLOBOCAN estimates of incidence and mortality worldwide for 36 cancers in 185 countries. CA Cancer J Clin 68:394–424.

BURONI FE, PERSICO MG, PASI F, LODOLA L, NANO R, APRILE C (2016) Radium-

223: Insight and Perspectives in Bone-metastatic Castration-resistant Prostate Cancer. Anticancer Res 36:5719–5730

Carter BS, Beaty TH, Steinberg GD, Childs B, Walsh PC (1992) Mendelian inheritance of familial prostate cancer. Proc Natl Acad Sci U S A 89:3367–3371.

Carvajal CE C-, Q L, A G (2012) Three-Dimensional Cell Culture Models for Biomarker Discoveries and Cancer Research. Transl Med Suppl1:1–8.

Castro E, Eeles R (2012) The role of BRCA1 and BRCA2 in prostate cancer. Asian J Androl 14:409–414.

Chakraborty S, Das T, Sarma HD, Venkatesh M, Banerjee S (2008) Comparative studies of 177Lu-EDTMP and 177Lu-DOTMP as potential agents for palliative radiotherapy of bone metastasis. Appl Radiat Isot 66:1196–1205.

Chandrasekaran S, Geng Y, DeLouise LA, King MR (2012) Effect of homotypic and heterotypic interaction in 3D on the E-selectin mediated adhesive properties of breast cancer cell lines. Biomaterials 33:9037–9048.

Chen N, Zhou Q (2016) The evolving Gleason grading system. Chinese J Cancer Res 28:58–64.

Costa EC, Moreira AF, de Melo-Diogo D, Gaspar VM, Carvalho MP, Correia IJ (2016) 3D tumor spheroids: an overview on the tools and techniques used for their analysis. Biotechnol Adv 34:1427–1441.

Cukierman E, Pankov R, Stevens DR, Yamada KM (2001) Taking cell-matrix adhesions to the third dimension. Science (80-) 294:1708–1712.

Daly T, Be H, Am S, Dp F (2017) Dose-escalated radiotherapy for clinically localised and locally advanced prostate cancer (Protocol). 2017:1–14.

Deshayes E, Roumiguie M, Thibault C, Beuzeboc P, Cachin F, Hennequin C, Huglo D, Rozet F, Kassab-Chahmi D, Rebillard X, Houédé N (2017) Radium 223 dichloride for prostate cancer treatment. Drug Des Devel Ther 11:2643–2651

Domińska K, Ochędalski T, Kowalska K, Matysiak-Burzyńska ZE, Płuciennik E, Piastowska-Ciesielska AW (2016) Interaction between angiotensin II and relaxin 2 in

the progress of growth and spread of prostate cancer cells. Int J Oncol 48:2619–2628.

Dowd FJ, Johnson BS, Mariotti AJ, Kwok KK, Vincent EC, Gibson JN (2017) Antineoplastic Drugs. Pharmacol Ther Dent:530–562

Drake RL, Vogl AW, Mitchell AW. (2015) Gray's Anatomy for Students, Third Edition.

Du Y, Carrio I, De Vincentis G, Fanti S, Ilhan H, Mommsen C, Nitzsche E, Sundram F, Vogel W, Oyen W, Lewington V (2017) Practical recommendations for radium-223 treatment of metastatic castration-resistant prostate cancer. Eur J Nucl Med Mol Imaging 44:1671–1678.

Dunn MW, Kazer MW (2011) Prostate cancer overview. Semin Oncol Nurs 27:241–250.

Eeles R, Raghallaigh HN (2018) Men with a susceptibility to prostate cancer and the role of genetic based screening. Transl Androl Urol 7:61–69.

Eger A, Mikulits W (2005) Models of epithelial–mesenchymal transition. Drug Discov Today Dis Model 2:57–63

Eilenberger C, Rudi S, Kratz A, Rothbauer M, Ehmoser E-K, Ertl P, Küpcü S (2018) Optimized alamarBlue assay protocol for drug dose-response determination of 3D tumor spheroids. MethodsX 5:781–787.

Elmore S (2007) Apoptosis: a review of programmed cell death. Toxicol Pathol 35:495–516

European Medicines Agency (EMA) (2014) Xofigo 1100 kBq/ml solución inyectable. Agencia Eur Medicam.

Ewing CM et al. (2012) Germline Mutations in HOXB13 and Prostate-Cancer Risk. N Engl J Med 366:141–149.

Fizazi K, Beuzeboc P, Lumbroso J, Haddad V, Massard C, Gross-Goupil M, Di Palma M, Escudier B, Theodore C, Loriot Y, Tournay E, Bouzy J, Laplanche A (2009) Phase II trial of consolidation docetaxel and samarium-153 in patients with bone metastases from castration-resistant prostate cancer. J Clin Oncol 27:2429–2435.

Friedl P, Wolf K (2003) Tumour-cell invasion and migration: diversity and escape mechanisms. Nat Rev Cancer 3:362–374

Friedrich J, Seidel C, Ebner R, Kunz-Schughart LA (2009) Spheroid-based drug screen: considerations and practical approach. Nat Protoc 4:309–324

Fujita K, Nonomura N (2018a) Role of Androgen Receptor in Prostate Cancer: A Review. World J Mens Health 36:1–8

Fujita K, Nonomura N (2018b) Role of Androgen Receptor in Prostate Cancer: A Review. World J Mens Health 36:1–8

Gay HA, Michalski JM (2018) Radiation Therapy for Prostate Cancer. Mo Med 115:146–150

Gebhard C, Gabriel C, Walter I (2016) Morphological and Immunohistochemical Characterization of Canine Osteosarcoma Spheroid Cell Cultures. Anat Histol Embryol 45:219–230

Haisler WL, Timm DM, Gage JA, Tseng H, Killian TC, Souza GR (2013) Three-dimensional cell culturing by magnetic levitation. Nat Protoc 8:1940–1949.

Harris WP, Mostaghel EA, Nelson PS, Montgomery B (2009) Androgen deprivation therapy: Progress in understanding mechanisms of resistance and optimizing androgen depletion. Nat Clin Pract Urol 6:76–85.

Harrison, George D, Wong, Armstrong A (2013) Radium-223 chloride: a potential new treatment for castration-resistant prostate cancer patients with metastatic bone disease. Cancer Manag Res 5:1–14

He J, Liang X, Luo F, Chen X, Xu X, Wang F, Zhang Z (2016) P53 Is Involved in a Three-Dimensional Architecture-Mediated Decrease in Chemosensitivity in Colon Cancer. J Cancer 7:900–909

Hoarau-Véchot J, Rafii A, Touboul C, Pasquier J (2018) Halfway between 2D and animal models: Are 3D cultures the ideal tool to study cancer-microenvironment interactions? Int J Mol Sci 19:181.

Huggins C, Hodges C V. (1941) Studies on prostatic cancer i. the effect of castration, of estrogen and of androgen injection on serum phosphatases in metastatic carcinoma of the prostate. Cancer Res 22:232–240.

Jacene H, Gomella L, Yu EY, Rohren A (2018) Hematologic Toxicity From Radium-223 Therapy for Bone Metastases in Castration-Resistant Prostate Cancer: Risk Factors and Practical Considerations. Clin Genitourin Cancer 16:919–926.

Jaganathan H, Gage J, Leonard F, Srinivasan S, Souza GR, Dave B, Godin B (2014) Three-Dimensional In Vitro Co-Culture Model of Breast Tumor using Magnetic Levitation. 4:1–9.

Kairemo K, Rohren EM, Anderson PM, Ravizzini G, Rao A, Macapinlac HA, Subbiah V (2019) Development of sodium fluoride PET response criteria for solid tumours (NAFCIST) in a clinical trial of radium-223 in osteosarcoma: from RECIST to PERCIST to NAFCIST. ESMO Open 4:e439

Kapałczyńska M, Kolenda T, Przybyła W, Zajączkowska M, Teresiak A, Filas V, Ibbs M, Bliźniak R, Łuczewski Ł, Lamperska K (2018) 2D and 3D cell cultures – a comparison of different types of cancer cell cultures. Arch Med Sci 14:910–919.

Kumar RJ, Barqawi A, Crawford ED (2005) Adverse events associated with hormonal therapy for prostate cancer. Rev Urol 7:S34–S45.

Lassi K, Dawson NA (2009) Emerging therapies in castrate-resistant prostate cancer. Curr Opin Oncol 21:260–265

Lassmann M, Eberlein U (2018) Targeted alpha-particle therapy: imaging, dosimetry, and radiation protection. Ann ICRP 47:187–195.

Lewington VJ (2005) Bone-seeking radionuclides for therapy. J Nucl Med Suppl1:34–47.

Li LT, Jiang G, Chen Q, Zheng JN (2015) Ki67 is a promising molecular target in the diagnosis of cancer (Review). Mol Med Rep 11:1566–1572

Liberal FDCG, Tavares AAS, Tavares JMRS (2017) Computational modeling of radiobiological effects in bone metastases for different radionuclides. Int J Radiat Biol 93:627–636

Liggett WH, Sidransky D (1998) Role of the p16 tumor suppressor gene in cancer. J Clin Oncol 16:1197–1206

Lopes PM, Sepúlveda L, Ramos R, Sousa P (2015) The role of transrectal ultrasound in the

diagnosis of prostate cancer: new contributions. Radiol Bras 48:7–11.

Marques I (2016) Rádio-223 no tratamento do carcinoma da próstata metastático. Available at: https://estudogeral.sib.uc.pt/bitstream/10316/36430/1/Tese Ines Marques %282016%29.pdf.

Marques IA, Neves AR, Abrantes AM, Pires AS, Tavares-da-Silva E, Figueiredo A, Botelho MF (2018) Targeted alpha therapy using Radium-223: From physics to biological effects. Cancer Treat Rev 68:47–54.

McNeal JE (1981) The zonal anatomy of the prostate. Prostate 2:35–49.

Mendes F, Sales T, Domingues C, Schugk S, Abrantes AM, Gonçalves AC, Teixo R, Silva R, Casalta-Lopes J, Rocha C, Laranjo M, Simões PC, Sarmento Ribeiro AB, Botelho MF, Rosa MS (2015) Effects of X-radiation on lung cancer cells: the interplay between oxidative stress and P53 levels. Med Oncol 32:266.

Mittler F, Obeïd P, Rulina A V, Haguet V, Gidrol X, Balakirev MY (2017) High-Content Monitoring of Drug Effects in a 3D Spheroid Model. Front Oncol 11:293

Monazzam A, Josephsson R, Blomqvist C, Carlsson J, Långström B, Bergström M (2007) Application of the multicellular tumour spheroid model to screen PET tracers for analysis of early response of chemotherapy in breast cancer. Breast Cancer Res 9:R45

Moore K (2013) Moore: Clinically Oriented Anatomy - 7th international ed, 7th ed.

Moses C, Garcia-Bloj B, Harvey AR, Blancafort P (2018) Hallmarks of cancer: The CRISPR generation. Eur J Cancer 93:10–18.

Mottet N, Bastian PJ, Bellmunt J, Van den Bergh RCN, Bolla M, Van Casteren NJ, Cornford P, Joniau S, Mason MD, Matveev V (2014) Guidelines on prostate cancer. Eur Urol.

Muz B, de la Puente P, Azab F, Azab AK (2015) The role of hypoxia in cancer progression, angiogenesis, metastasis, and resistance to therapy. Hypoxia 11:83–92

Nyga A, Cheema U, Loizidou M (2011) 3D tumour models: Novel in vitro approaches to cancer studies. J Cell Commun Signal 5:239–248.

Odo U, Vasudevamurthy AK, Sartor O (2017) Acute Promyelocytic Leukemia After

Treatment of Metastatic Castration-Resistant Prostate Cancer With Radium-223. Clin Genitourin Cancer 15:e501–e502

Ohori M, Dunn JK, Scardino PT (1995) Is prostate-specific antigen density more useful than prostate-specific antigen levels in the diagnosis of prostate cancer? Urology 46:666–671.

Orellana E, Kasinski A (2016) Sulforhodamine B (SRB) Assay in Cell Culture to Investigate Cell Proliferation. BIO-PROTOCOL 6:e1984.

Ottewell PD, Wang N, Meek J, Fowles CA, Croucher PI, Eaton CL, Holen I (2014) Castration-induced bone loss triggers growth of disseminated prostate cancer cells in bone. Endocr Relat Cancer 21:769–781.

Pallwein L, Mitterberger M, Pelzer A, Bartsch G, Strasser H, Pinggera GM, Aigner F, Gradl J, zur Nedden D, Frauscher F (2008) Ultrasound of prostate cancer: Recent advances. Eur Radiol 18:707–715.

Parker C et al. (2013) Alpha Emitter Radium-223 and Survival in Metastatic Prostate Cancer. N Engl J Med 369:213–223

Parker C, Heidenreich A, Nilsson S, Shore N (2018) Current approaches to incorporation of radium-223 in clinical practice. Prostate Cancer Prostatic Dis 21:37–47.

Patel AR, Klein EA (2009) Risk factors for prostate cancer. Nat Clin Pract Urol 6:87–95.

Pilie P, Giri V, Cooney K (2016) HOXB13 and other high penetrant genes for prostate cancer. Asian J Androl 18:530–532.

Porter SN, Baker LC, Mittelman D, Porteus MH (2014) Lentiviral and targeted cellular barcoding reveals ongoing clonal dynamics of cell lines in vitro and in vivo. Genome Biol 15:1–14.

Powell IJ, Bollig-Fischer A (2013) Minireview: The Molecular and Genomic Basis for Prostate Cancer Health Disparities. Mol Endocrinol 27:879–891.

Pu X, Storr SJ, Zhang Y, Rakha EA, Green AR, Ellis IO, Martin SG (2017) Caspase-3 and caspase-8 expression in breast cancer: caspase-3 is associated with survival. Apoptosis 22:357–368

Rampersad SN (2012) Multiple applications of alamar blue as an indicator of metabolic function and cellular health in cell viability bioassays. Sensors (Switzerland) 12:12347–12360.

Riffle S, Pandey RN, Albert M, Hegde RS (2017) Linking hypoxia, DNA damage and proliferation in multicellular tumor spheroids. BMC Cancer 17:1–12

Ritch CR, Cookson MS (2016) Advances in the management of castration resistant prostate cancer. BMJ.

Roato I (2013) Interaction among Cells of Bone, Immune System, and Solid Tumors Leads to Bone Metastases. Clin Dev Immunol 2013:1–7.

Rodrigues S, Dores M, Metrogos V, Rodrigues M, Neto Gomes P, Cabrita M, Rosa G, Coutinho A, Neves J (2014) Carcinoma da próstata metastático resistente à castração - novas abordagens terapêuticas. Acta Urológica Port 31:36–40

Rodríguez SA, Arias Fúnez F, Bueno Bravo C, Rodríguez-Patrón Rodríguez R, Sanz Mayayo E, Palacios VH, Burgos Revilla FJ (2014) Cryotherapy for Primary Treatment of Prostate Cancer: Intermediate Term Results of a Prospective Study from a Single Institution. Prostate Cancer 2014:1–11.

Saad F, Hotte SJ (2010) Guidelines for the management of castrate-resistant prostate cancer. J Can Urol Assoc 4:380–384.

Sabattini S, Renzi A, Marconato L, Militerno G, Agnoli C, Barbiero L, Rigillo A, Capitani O, Tinto D, Bettini G (2018) Comparison between May-Grünwald-Giemsa and rapid cytological stains in fine-needle aspirates of canine mast cell tumour: Diagnostic and prognostic implications. Vet Comp Oncol 16:511–517.

Sant S, Johnston PA (2017) The production of 3D tumor spheroids for cancer drug discovery. Drug Discov Today Technol 23:27–36

Satelli A, Li S (2011) Vimentin in cancer and its potential as a molecular target for cancer therapy. Cell Mol Life Sci 68:3033–3046

Sathianathen NJ, Konety BR, Crook J, Saad F, Lawrentschuk N (2018) Landmarks in prostate cancer. Nat Rev Urol 15:627–642.

Sekhon N, Kumbla RA, Mita M (2017) Current Trends in Cancer Therapy. In: Cardio-Oncology, pp 1–24. Elsevier.

Sgouros G (2008) Alpha-particles for targeted therapy. Adv Drug Deliv Rev 60:1402–1406.

Shafi AA, Yen AE, Weigel NL (2013) Androgen receptors in hormone-dependent and castration-resistant prostate cancer. Pharmacol Ther 140:223–238.

Shen MM, Abate-Shen C (2010) Molecular genetics of prostate cancer: New prospects for old challenges. Genes Dev 24:1967–2000.

Singh S, Sadacharan S, Su S, Belldegrun A, Persad S, Singh G (2003) Overexpression of Vimentin: Role in the Invasive Phenotype in an Androgen-independent Model of Prostate Cancer 1. Cancer Res 63:2306–2311

Sleeboom JJF, Eslami Amirabadi H, Nair P, Sahlgren CM, den Toonder JMJ (2018) Metastasis in context: modeling the tumor microenvironment with cancer-on-a-chip approaches. Dis Model Mech 11

Smith M, Parker C, Saad F, Miller K, Tombal B, Ng QS, Boegemann M, Matveev V, Piulats JM (2019) Addition of radium-223 to abiraterone acetate and prednisone or prednisolone in patients with castration-resistant prostate cancer and bone metastases (ERA 223): a randomised , double-blind , placebo-controlled , phase 3 trial. Lancet Oncol 2045:1–12.

Souza GR, Molina JR, Raphael RM, Ozawa MG, Stark DJ, Levin CS, Bronk LF, Ananta JS, Mandelin J, Georgescu M-M, Bankson JA, Gelovani JG, Killian TC, Arap W, Pasqualini R (2010) Three-dimensional tissue culture based on magnetic cell levitation. Nat Nanotechnol 5:291–296

Subbiah V, Anderson PM, Kairemo K, Hess KR, Huh WW, Ravi V, Daw NC, Somaiah N, Ludwig JA, Benjamin RS, Chawla SP, Hong DS, Meric-Bernstam F, Ravizzini G, Kleinerman ES, Macapinlac HA, Rohren EM (2019) Alpha particle Radium 223 dichloride in high-risk osteosarcoma: a phase I dose escalation trial. Clin Cancer Res 2018:964

Tan ME, Li J, Xu HE, Melcher K, Yong EL (2015) Androgen receptor: Structure, role in

prostate cancer and drug discovery. Acta Pharmacol Sin 36:3–23.

Toufektchan E, Toledo F (2018) The Guardian of the Genome Revisited: p53 Downregulates Genes Required for Telomere Maintenance, DNA Repair, and Centromere Structure. Cancers (Basel) 10

Tran C, Ouk S, Clegg NJ, Chen Y, Watson PA, Arora V, Wongvipat J, Smith-Jones PM, Yoo D, Kwon A, Wasielewska T, Welsbie D, Chen CD, Higano CS, Beer TM, Hung DT, Scher HI, Jung ME, Sawyers CL (2009) Development of a Second-Generation Antiandrogen for Treatment of Advanced Prostate Cancer. Science (80-) 324:787–790

Tsao C-K, Cutting E, Martin J, Oh WK (2014) The role of cabazitaxel in the treatment of metastatic castration-resistant prostate cancer. Ther Adv Urol 6:97–104

van Zijl F, Krupitza G, Mikulits W (2011) Initial steps of metastasis: cell invasion and endothelial transmigration. Mutat Res 728:23–34

Vichai V, Kirtikara K (2006) Sulforhodamine B colorimetric assay for cytotoxicity screening. Nat Protoc 1:1112–1116.

Wang G, Zhao D, Spring DJ, Depinho RA (2018) Genetics and biology of prostate cancer. Genes Dev 32:1105–1140.

Wang MC, Valenzuela LA, Murphy GP, Chu TM (2017) Purification of a Human Prostate Specific Antigen. J Urol 17:159–163.

Wlodkowic D, Skommer J, Darzynkiewickz Z (2009) Flow cytometry-based apoptosis detection. Methods Mol Biol 559:1–14.